

RICE UNIVERSITY

Influence of Uncertainties in Vertical Mixing Algorithms

on an Air Quality Model

by

Wei Tang

A THESIS SUBMITTED

IN PARTIAL FULFILLMENT OF THE

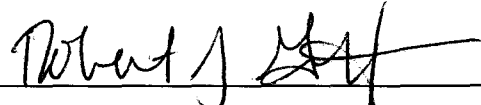
REQUIREMENTS FOR THE DEGREE

Master of Science

APPROVED, THESIS COMMITTEE:



Daniel S. Cohan, Assistant Professor, Chair
Civil and Environmental Engineering



Robert J. Griffin, Associate Professor
Civil and Environmental Engineering



Philip B. Bedient, Professor
Civil and Environmental Engineering

HOUSTON, TEXAS

JANUARY 2010

UMI Number: 1485973

All rights reserved

INFORMATION TO ALL USERS

The quality of this reproduction is dependent upon the quality of the copy submitted.

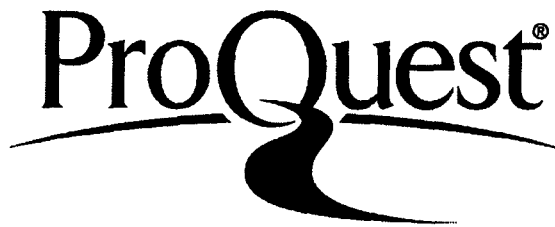
In the unlikely event that the author did not send a complete manuscript and there are missing pages, these will be noted. Also, if material had to be removed, a note will indicate the deletion.



UMI 1485973

Copyright 2010 by ProQuest LLC.

All rights reserved. This edition of the work is protected against unauthorized copying under Title 17, United States Code.



ProQuest LLC
789 East Eisenhower Parkway
P.O. Box 1346
Ann Arbor, MI 48106-1346

ABSTRACT

Influence of Uncertainties in Vertical Mixing Algorithms on an Air Quality Model

by

Wei Tang

Vertical diffusion of trace pollutants is a very important physical process that influences pollutant concentrations. However, there are large uncertainties in the numerical modeling of this process, which could affect model predictions of pollutant levels and their responsiveness to emission controls. Uncertainties could result from the formulation of vertical diffusion schemes or from errors in eddy diffusivity and dry deposition velocity parameters associated with this process. Inter-comparisons between different model configurations and sensitivity analysis of model parameters can be used to help quantify these uncertainties. In this study, a comprehensive evaluation of two vertical diffusion schemes, EDDY and ACM2, was performed by comparing ground-level concentrations and vertical profiles generated using the CMAQ model with measurement data from the Texas Air Quality Study II. In addition, new capabilities of conducting sensitivity analysis to dry deposition velocity and eddy diffusivity were implemented into the CMAQ-DDM model. The results show that the ACM2 scheme tends to predict larger secondary pollutant concentrations and smaller primary pollutant concentrations at the surface compared to the EDDY scheme. Differences between the two vertical diffusion schemes and uncertainties in dry deposition velocity may cause temporal variations in the responsiveness of ozone to both NO_x and VOC control respectively.

ACKNOWLEDGEMENTS

I would like express my deepest appreciation to my advisor Dr. Daniel Cohan, for giving me this opportunity to work in this exciting environmental field, and his support, understanding, trust, encouragement, and insightful guidance throughout the whole study. I am also grateful to my committee members, Dr. Robert Griffin and Dr. Philip Bedient, for concerning about my research progress and taking the time to serve on my thesis committee, and their dedication and persistence helped me understand my topic, both, conceptually and theoretically.

I sincerely appreciate the whole-hearted help given by my colleagues, Dr. Xue Xiao, Wei Zhou, and Antara Digar throughout my research, without their help, I could not make it. I am also thankful to Dr. Gary Morris from Valparaiso University, for providing ozonesondes data and helpful discussions along the way. I also want to thank Dr. Sergey Napelenok at US EPA, the air quality research team at University of Houston, and the staffs at our department for their help.

I would like to give my sincerest gratitude to my family, for their tremendous love, blessing, and support throughout this journey.

Finally, I gratefully acknowledge the financial support for this project from the U.S. Environmental Protection Agency (EPA) and Texas Environmental Research Consortium (TERC).

Table of Contents

	Page
List of Tables.....	vi
List of Figures.....	vii
Nomenclature.....	x
Chapter	
Introduction.....	1
References.....	6
Background and Literature Review.....	10
2.1 Tropospheric ozone pollution in Houston.....	10
2.2 Community Multiscale Air Quality Modeling System (CMAQ).....	12
2.3 Vertical diffusion schemes in CMAQ.....	14
2.4 Vertical eddy diffusivity (K_z).....	18
2.5 Dry deposition velocity (V_d).....	19
2.6 DDM-3D sensitivity analysis.....	25
References.....	31
Methodology.....	36
3.1 Model development.....	36
3.1.1 Crank-Nicolson scheme.....	36
3.1.2 Numerical implementation.....	38
3.1.3 Accuracy test.....	41
3.2 Model evaluation.....	42
3.2.1 Model configurations.....	42
3.2.2 Data comparisons.....	44

3.3 Sensitivity and Uncertainty analysis.....	46
3.3.1 Sensitivity analysis	47
3.3.2 Uncertainty in dry deposition velocity	48
References.....	51
Results and Discussions.....	52
4.1 Accuracy test results.....	52
4.2 Vertical diffusion schemes evaluation.....	57
4.2.1 Regional ozone modeling	58
4.2.2 EDDY and ACM2 modeling data comparisons	60
4.2.3 Comparison with surface measurements	63
4.2.4 Comparison with ozonesonde measurements.....	68
4.2.5 Comparison with regional aircraft measurements	71
4.3 Sensitivity analysis	74
4.4 Uncertainty analysis in dry deposition velocity.....	80
4.4.1 Effect on model simulations	80
4.4.2 Effect on emission control strategy	83
References.....	89
Conclusions and Recommendations	91
5.1 Conclusions	91
5.2 Recommendations for future work	93

LIST OF TABLES

Tables	Page
3.1: CMAQ science options	44
4.1: Sensitivity coefficients of 1-hr ozone with respect to dry deposition velocity, eddy diffusivity, and emission, and statistical consistency of Brute Force and DDM-3D results	56
4.2: Effects of uncertainties on emission control (Deer Park)	86
4.3: Effects of uncertainties on emission control (Bayland Park)	87

LIST OF FIGURES

Figure	Page
2.1: TexAQS 2000 and TexAQS II field studies area	11
2.2: Science process modules in Model-3 CMAQ	13
2.3: Schematic representation of the exchange among model layers in three schemes	15
2.4: Resistance model for dry deposition	20
2.5: Schematic diagram of pathway resistances used in RADM method	22
2.6: Schematic diagram of pathway resistances used in M3DDEP method	24
2.7: Schematic ozone responses to emission, and BF and DDM-3D sensitivities	29
3.1: Moeling domain of East Texas	42
3.2: SMOKE emissions processing	43
3.3: Field measurement locations and surface sites inside modeling domain	45
4.1a: Sensitivity coefficients from DDM and Brute Force of EDDY scheme at time of peak ozone (4:00PM CST) on August 31 st , 2006	53
4.1b: Sensitivity coefficients from DDM and Brute Force of ACM2 scheme at time of peak ozone (4:00PM CST) on August 31 st , 2006	54
4.2: Eastern Texas county map and HGB ozone non-attainment area	58
4.3: Wind conditions and PBL height at ozone peak time (4:00PM CST) on August 31 st , 2006	59
4.4: Ozone concentration at peak time (4:00PM CST) on August 31 st , 2006	59
4.5: Regression between 1-hr average pollutant concentrations for all days in the episode modeled using EDDY and those modeled using ACM2	61

4.6: Vertical profiles produced by EDDY and ACM2 schemes for NO _x and O ₃ mixing ratios averaged over 4pm to 10pm on August 31 st , 2006 in Houston	62
4.7: Scatter diagram of modeled 1-hr O ₃ versus observed data	64
4.8: Time series (UTC) of predicted and observed ozone at four sites	65
4.9: Time series (UTC) of predicted and observed NO _x at four sites	66
4.10: Time series (UTC) of predicted and observed CO at four sites	67
4.11a: Measured and modeled data for ozonesondes launched from University of Houston	69
4.11b: Measured and modeled data for ozonesondes launched from NOAA R.H Brown vessel	70
4.12: P-3 aircraft track at 3:00pm on August 31 st , 2006	72
4.13: Modeled and P-3 aircraft data for O ₃ , NO _x , and CO	72
4.14a: Ozone sensitivity to dry deposition velocity at 4:00pm (CST) on August 31 st , 2006	75
4.14b: Responsiveness of ozone to dry deposition velocity at 4:00pm (CST)	75
4.15a: Ozone concentration at peak time (4:00PM CST) on August 31 st , 2006	76
4.15b: Ozone sensitivities to anthropogenic NO _x and VOC at peak time 4:00pm (CST) on August 31 st , 2006	76
4.16: Cross sensitivity coefficients of ozone to dry deposition velocity and anthropogenic NO _x , and anthropogenic VOC at 4:00pm on August 31 st , 2006	79
4.17: Effect of uncertainty in O ₃ dry deposition velocity on surface O ₃ modeling	81
4.18a: Effect of uncertainty in dry deposition velocity on O ₃ vertical profile	82

4.18b: Effects of uncertainty in dry deposition velocities on HNO ₃ and SO ₂ vertical profiles	83
4.19: Effects of uncertainty in different vertical mixing schemes on O ₃ sensitivity to anthropogenic NO _x , to anthropogenic VOC emissions	84
4.20: Effects of uncertainty in dry deposition velocity on O ₃ sensitivity to anthropogenic NO _x , to anthropogenic VOC emissions	85

NOMENCLATURE

Abbreviations

ACM	Asymmetric Convective Model
CMAQ	Community Multiscale Air Quality Modeling System
CCTM	CMAQ Chemistry-Transport Model
(H)DDM	(High order) Decoupled Direct Method
EDDY	Eddy Diffusion Model
EPA	Environmental Protection Agency
GoMACCS	Gulf of Mexico Atmospheric Composition and Climate Study
HGB	Houston Galveston Brazoria
ION-6	Intercontinental Transport Experiment Ozonesonde Network Study 2006
M3DDEP	Model-3 DRY Deposition Model
MCIP	Meteorology-Chemistry Interface Processor
MM5	Fifth Generation Mesoscale Meteorological Model
NOAA	National Oceanic and Atmospheric Administration
NAAQS	National Ambient Air Quality Standards
NEI	National Emission Inventory
NO _x	Nitrogen Oxides
NetCDF	Network Common Data Format
PBL	Planetary Boundary Layer
PPM	Piecewise Parabolic Method
RADM	Regional Acid Deposition Model
SIP	State Implementation Plan

SMOKE Sparse Matrix Operator Kernel Emissions Model
TCEQ Texas Commission for Environmental Quality
TexAQS II Texas Air Quality Study II
VOC Volatile Organic Compounds

Symbols

Δz thickness of layer
 K_z eddy diffusivity
 f_{conv} partitioning factor
 k von Karman constant
 h PBL height
 L Monin-Obukov Length scale
 Pr_0 Prandtl number of neutral stability
 β_h coefficients of profile functions for heat
 γ_h coefficients of profile functions for heat
 u^* friction velocity
 w^* convective velocity
 z reference height
 z_1 height of first model layer
 z_0 roughness length
 V_d dry deposition velocity
 R_a aerodynamic resistance

R_{bh}	Quasi laminar boundary layer resistance for heat
R_{bx}	Quasi laminar boundary layer resistance for trace species
R_c	Canopy resistance
R_s	Surface resistance
Sc	Schmidt number
z_{SL}	surface layer height
z_{dep}	deposition height
r_{sx}	stomatal resistance
r_{mx}	mesophyl resistance
r_{lux}	resistance of the outer surface of leaves in the upper canopy
r_{dc}	resistance for the gas transfer affected by buoyant convection in canopy
r_{clx}	lower canopy resistance
r_{ac}	resistance that depends on the canopy height
r_{gsx}	resistance of soil, leaf litter
Θ_g	potential temperature of the air
Θ_l	potential temperature of the ground surface
r_{stb}	bulk stomatal resistance
r_{st}	stomatal resistance on a leaf layer
r_m	mesophyl resistance
r_{cut}	dry cuticle resistance
r_{cw}	wet cuticle resistance
r_g	ground resistance
r_{lc}	in-canopy aerodynamic resistance

f_v	vegetation fractional coverage
f_w	fractional leaf area wetness
LAI	leaf area index
p	a sensitivity parameter
P	unperturbed (base case) value of parameter p
ppb	parts per billion
ppm	parts per million
ϵ	scaling variable for a sensitivity parameter (nominal value 1)
$\Delta\epsilon$	fractional change in a sensitivity parameter
E	emissions
$S_j^{(1)}$	first-order semi-normalized sensitivity coefficients
$S_{j,k}^{(2)}$	second-order semi-normalized sensitivity coefficients

CHAPTER 1

Introduction

Air quality models are very useful tools in air quality management and atmospheric science studies. They are applied by scientists and policy makers to get a better understanding of the fate and transport of air pollutants and to develop emission control strategies in order to protect human health and mitigate environmental impacts (Carmichael et al., 1991; McKeen et al., 1991; Lu et al., 1997; Bouchet et al., 1999; Kasibhatla and Chameides, 2000). However, due to physical parameterizations, large data requirements, and numerical approximations in air quality modeling, uncertainties cannot be eliminated and may have a significant impact on model performance (Pinder et al., 2009; Zhang et al., 2007; Mallet and Sportisse, 2006). Hence, quantifying the effects of these uncertainties on the model predicted results is essential not only for model validation but also for scientific research and air quality policy analysis. In order to do so, uncertainty analysis is required (Cacuci, 2003).

Structural uncertainty and parametric uncertainty are two types of uncertainties in air quality models. Structural uncertainty results from a lack basic knowledge of fundamental mechanisms in model configurations, such as chemical mechanisms, transport mechanisms, or planetary boundary layer mechanisms. Parametric uncertainty is from measurement error, statistical sampling error, or parameterization error in the model inputs and parameters, such as emission inventories, dry deposition velocities, or eddy diffusivity

(Pinder et al., 2009; Mallet and Sportisse, 2006; Ozkaynak et al., 2009). These uncertainties would be problematic for the model simulation and policy decision making because they may cause variations and inaccuracies in model outputs. To assess structural uncertainties, an ensemble approach, which includes multiple model runs of a single event through inter-comparisons between varied model configurations, typically is used (Pinder et al., 2009; Mallet and Sportisse, 2006). To estimate parametric uncertainties, sensitivity analysis can be used to help characterize the response of concentrations to model input errors and model parameter errors (Pinder et al., 2009).

Sensitivity analysis is a method used to evaluate the impact of parameter variations on calculated results (Cacuci, 2003). Sensitivity coefficients calculated via sensitivity analysis are used to determine quantitatively the response of model prediction to the input parameter's variation. Numerous methods, such as Brute Force, Green's Function Method (GFM), Automatic Differentiation in Fortran (ADIFOR), and Decoupled Direct Method (DDM) have been developed and used to calculate sensitivity coefficients. Compared to the other methods, DDM is more direct, efficient and stable, and is less subject to numerical noise. It has been used for many years and has been implemented into many models for sensitivity analysis (e.g., Yang et al., 1997; Hakami et al., 2003, 2004).

Vertical diffusion is a very important physical process in atmospheric models. However, studies by Pleim (2006a, 2006b) indicated that large uncertainties still remain in the numerical modeling of vertical transport of atmospheric properties and chemical

species, especially under the convective boundary layer in both meteorology and air quality models. Uncertainties could come from lack of knowledge in vertical transport mechanisms (structural) and/or from physical parameterization error in dry deposition velocity and eddy diffusivity (parametric), which are two very important parameters associated with vertical diffusion process (Hicks and Wesely, 2000; Wilson 2004).

The Community Multiscale Air Quality Modeling System (CMAQ) model is a third generation, three-dimensional Eulerian air quality model that simulates ozone, acid deposition, visibility, and fine particulate matter in the troposphere (Byun and Schere, 2006). It can simulate multiple pollutants simultaneously in various scales and was designated by the U.S. Environmental Protection Agency (U.S.EPA) for regulatory, policy analysis, and scientific investigation (CMAS 2009). The eddy diffusion scheme (EDDY) and a newly developed asymmetric convective model scheme (ACM2) are the two options for simulating vertical turbulent mixing in CMAQ. The EDDY scheme deals with turbulent mixing only in a sub-grid-scale, and the original ACM scheme considers turbulent mixing only in a super-grid-scale. The ACM2 scheme combines the above two turbulent mixing schemes, enabling the model to simulate vertical transport in both small and large scales (Pleim 2006a). In addition, the ACM2 scheme has recently replaced EDDY as default option in CMAQ. To evaluate the uncertainty in model configurations from using different vertical mixing schemes, comparisons between the modeling results from the two schemes as well as with observation data are required. Although a few

comparisons between EDDY and ACM2 schemes have been conducted previously (Pleim 2006, 2009), more comprehensive evaluations with different scenarios are still highly desirable.

Currently, the sensitivity of pollutant concentrations to initial conditions, boundary conditions, emissions, and reaction rate constants has been determined in CMAQ using DDM technique (Cohan et al., 2005; Jin et al., 2008). However, DDM has not been implemented previously into the newly developed ACM2 scheme, and capabilities of analyzing sensitivities to dry deposition velocity and eddy diffusivity have not been added into CMAQ-DDM. Hence, this model development work has enabled the CMAQ-DDM model to perform sensitivity analysis with the ACM2 scheme and also to calculate sensitivity coefficients for dry deposition velocity and eddy diffusivity in order to qualitatively and quantitatively investigate the parametric uncertainties in the model.

The major accomplishments of this study are: first, DDM was implemented into the ACM2 scheme; second, new features for calculating sensitivities to dry deposition velocity and to eddy diffusivity have been added into CMAQ-DDM; third, EDDY and ACM2 vertical diffusion schemes in CMAQ model were evaluated comprehensively using Texas Air Quality Study II field measurement data; fourth, sensitivity analysis was performed to investigate the effect of uncertainty in dry deposition velocity on predictions of pollutant concentrations and their sensitivities to emission change. Based on this study, the relative strengths of ACM2 and EDDY can be demonstrated, the effect of uncertainty in dry

deposition velocity on CMAQ model simulation can be examined, and the effect of uncertainty in dry deposition velocity on emission controls can be quantified.

In this thesis, Chapter Two reviews current knowledge and literature related to this study; Chapter Three demonstrates the methodology of this study. Chapter Four discusses finding and results from this study, and Chapter Five draws conclusions and recommends future work.

References

- Bouchet, V.S., Laprise, R., and Torlaschi, E. (1999) Studying ozone climatology with a regional climate model: 2. Climatology. *Journal of Geophysical Research*. 104, 30373–30385.
- Byun, D. and Schere, K.L. (2006) Review of the governing equations, computational algorithms, and other components of the Models-3 Community Multiscale Air Quality (CMAQ) modeling system. *Applied Mechanics Reviews*. 59, 51-77.
- Cacuci, D.G. (2003) *Sensitivity and uncertainty analysis*. Chapman & Hall/CRC, Boca Raton, Florida.
- Carmichael, G. R., Peters, L.K., and Saylor, R.D. (1991) The STEM-II regional-scale acid deposition and photochemical oxidant model, I. An overview of model developments and applications. *Atmospheric Environment*. 25A, 2077–2090.
- CMAS center. *CMAQ v4.6 operational guidance document*.
(http://www.cmaqmodel.org/op_guidance_4.6/index.cfm. Accessed on October 1st, 2009)
- Cohan D.S., Hakami, A., Hu, Y.T., and Russell, A.G. (2005) Nonlinear response of ozone to emissions: Source apportionment and sensitivity analysis. *Environmental Science and Technology*. 39, 6739-6748.

- Hakami, A., Odman, M.T., and Russell, A.G. (2003) High-order, direct sensitivity analysis of multidimensional air quality models. *Environmental Science and Technology*. 37, 2442-2452.
- Hakami, A., Odman, M.T., and Russell, A.G. (2004) Nonlinearity in atmospheric response: A direct sensitivity analysis approach. *Journal of Geophysical Research*. 109, D15303.
- Jin, L., Tonse, S., Cohan, D.S., Mao, XL., Harley, R.A., and Brown, N.J. (2008) Sensitivity analysis of ozone formation and transport for a central California air pollution episode. *Environmental Science and Technology*. 42, 3683-3689.
- Kasibhatla, P. and Chameides, W.L. (2000) Seasonal modeling of regional ozone pollution in the eastern United States. *Geophysical Research Letters*. 27, 1415–1418.
- Lu, R., Turco, R.P., and Jacobson M.Z. (1997) An integrated air pollution modeling system for urban and regional scales: 1. Structure and performance. *Journal of Geophysical Research*. 102, 6063–6079.
- Mallet, V. and Sportisse, B. (2006) Uncertainty in a chemistry-transport model due to physical parameterizations and numerical approximations: An ensemble approach applied to ozone modeling. *Journal of Geophysical Research*. 111, D01302.

- McKeen, S. A., Hsie, E.Y., Trainer, M., Tallamraju, R., and Liu, S.C. (1991) A regional model study of the ozone budget in the eastern United States. *Journal of Geophysical Research*. 96, 10809–10845.
- Ozkaynak, H., Frey, H.C., Burke, J., and Pinder, R.W. (2009) Analysis of coupled model uncertainties in source-to-dose modeling of human exposures to ambient air pollution: A PM_{2.5} case study. *Atmospheric Environment*. 43, 1641-1649.
- Pleim, J.E. (2006a) A combined local and nonlocal closure model for the atmospheric boundary layer. Part II: Application and evaluation in a mesoscale meteorological model. *Journal of Applied Meteorology and Climatology*. 46, 1396-1408.
- Pleim, J.E. (2006b) A new combined local and non-local PBL model for meteorology and air quality modeling. CMAS conference paper. North Carolina.
- Pleim, J.E. Planetary boundary layer modeling for meteorology and air quality. (http://www.epa.gov/AMD/peer/posters/Poster_1.6.pdf Accessed on September 16th, 2009)
- Pinder, R.W., Gilliam, R.C., Appel, K.W., Napelenok, S.L., Foley, K.M., and Gilliland, A.B. (2009) Efficient probabilistic estimates of surface ozone concentration using an ensemble of model configurations and direct sensitivity calculations. *Environmental Science and Technology*. 43, 2388-2393.

- Wesely, M.L. and Hicks, B.B. (2000) A review of the current status of knowledge on dry deposition. *Atmospheric Environment*. 34, 2261-2282.
- Wilson, R. (2004) Turbulent diffusivity in the free atmosphere inferred from MST radar measurements: A review. *Annales Geophysicae*. 22, 3869-3887.
- Yang, YJ., Wilkinson, J.G., and Russell, A.G. (1997) Fast, direct sensitivity analysis of multidimensional photochemical models. *Environmental Science and Technology*. 31, 2859-2868.
- Zhang, F. Q., Bei, N. F., Nielsen-Gammon, J. W., Li, G. H., Zhang, R. Y., Stuart, A., and Aksoy, A. (2007) Impacts of meteorological uncertainties on ozone pollution predictability estimated through meteorological and photochemical ensemble forecasts. *Journal of Geophysical Research*. 112, D04304.

CHAPTER 2

Background and Literature Review

This chapter reviews the current knowledge and scientific literature regarding air quality in Houston, the CMAQ model, vertical diffusion algorithms in CMAQ, vertical eddy diffusivity, dry deposition velocity, and the DDM-3D method for sensitivity calculation.

2.1 Tropospheric ozone pollution in Houston

Ozone in troposphere is formed through the reactions between nitrogen oxides (NO_x) and volatile organic compounds (VOCs) in the presence of sunlight (Seinfeld and Pandis, 2002). The Houston-Galveston-Brazoria (HGB) region located in southeast Texas and in proximity to Gulf of Mexico has five million inhabitants and the largest concentration of petrochemical facilities in the United States. The large sources of NO_x and VOC emissions and the meteorological conditions such as extended heat and humidity, and intense solar radiation makes HGB one of the worst ozone pollution region in the US; it has been classified by the U.S.EPA as an ozone non-attainment area (Kleinman et al., 2002; Ryerson et al., 2003; Daum et al., 2004; Rappengluck et al., 2008). Two intensive air quality study field campaigns were conducted in eastern Texas, as shown in Figure 2.1, to investigate the sources and the causes of ozone and aerosol formation in the atmosphere (Parrish et al., 2009). In addition to field measurements, air quality modeling studies also are performed to better understand atmospheric processes and air pollutants transport and to help the Texas Commission on Environmental Quality (TCEQ) establish the state implementation

plan (SIP) for complying with U.S. EPA National Ambient Air Quality Standards (NAAQS) (Byun et al. 2007).

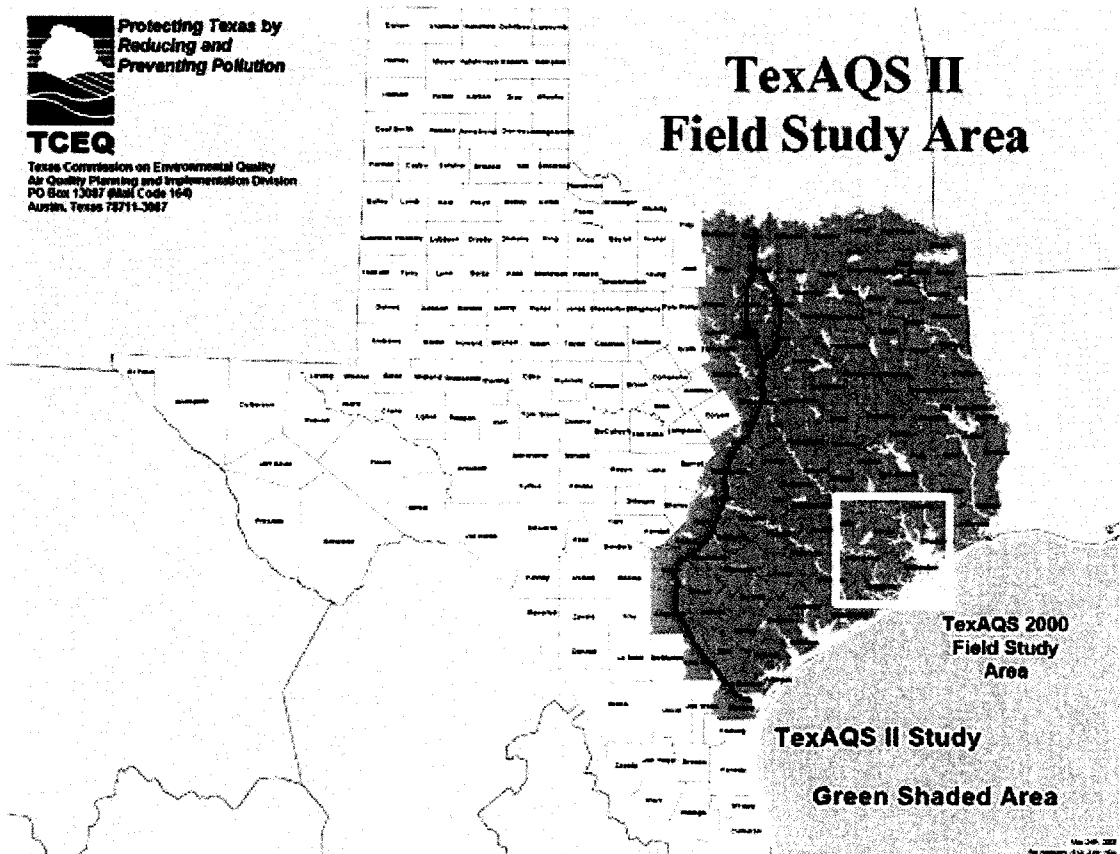


Figure 2.1: TexAQS 2000 and TexAQS II field studies area. (Source: TCEQ, 2009)

The Community Multiscale Air Quality Modeling System (CMAQ) model was used in this study to simulate an air pollution episode during August 30th to September 5th 2006 associated with TexAQS II air quality field study in eastern Texas.

2.2 Community Multiscale Air Quality Modeling System (CMAQ)

Community Multiscale Air Quality Modeling System (CMAQ) is an Eulerian air quality model and has been used to simulate ozone, acid deposition, visibility, and fine particulate matter in the troposphere for regulatory, policy analysis and scientific investigation (Byun and Schere, 2006). CMAQ separates a modeling domain into many grid cells and calculates the species concentrations affected by different atmospheric processes using operator splitting in each grid cell. The processes that were considered as main factors influencing the species concentrations include emissions from sources, horizontal and vertical advection, horizontal and vertical diffusion, chemical reaction, and deposition. The general governing equation for these processes is shown in equation 2.1.

$$\frac{dC}{dt} = [advection] + [diffusion] + [deposition] + [chemistry] + [emission] \quad (2.1)$$

The concentration calculations are conducted by the chemistry-transport model component of CMAQ (CCTM), which is the last program in CMAQ modeling sequence. The advection and emission terms as shown in equation 2.1 were calculated using input data generated by meteorology and emission models, and the deposition, chemical reaction, and diffusion terms were calculated inside the CCTM (CMAS, 2009). The model framework is shown in Figure 2.2.

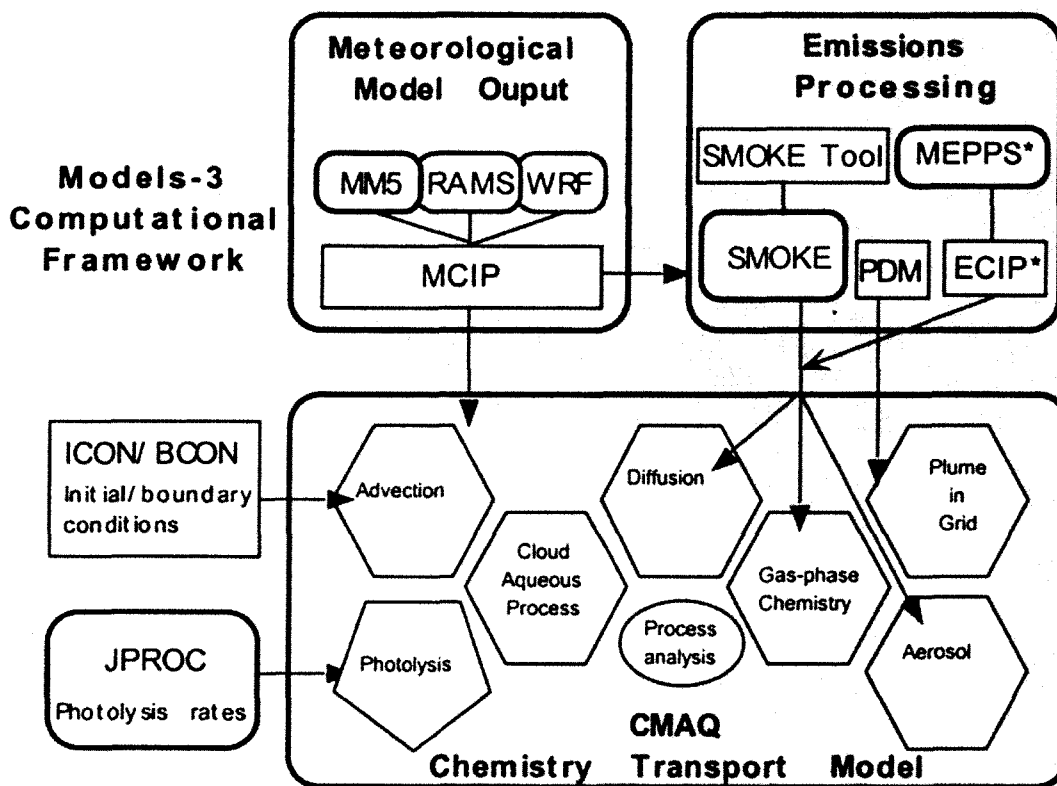


Figure 2.2: Science process modules in Model-3 CMAQ. (Source: Byun and Schere, 2006)

To solve the continuity equation 2.1, initial and boundary condition are required. The initial and boundary conditions for the CMAQ model simulation were generated by the initial condition preprocessor, ICON, and boundary condition preprocessor, BC0N, as shown in Figure 2.2. In Figure 2.2, the photolysis rate preprocessor, JPROC, calculates photolysis rate constants that can be used by CCTM to simulate photolysis reactions; the Meteorology-Chemistry interface preprocessor, MCIP, converts meteorology data generated by a meteorology model such as Fifth Generation Mesoscale Meteorological Model, MM5, and Weather Research Forecasting Model, WRF, to a CMAQ-ready

meteorology field. The Sparse Matrix Operator Kernel Emission Model, SMOKE, generates CMAQ-ready emission files (Byun and Schere, 2006; CMAS 2009).

As shown in Figure 2.2, diffusion is one of physical processes simulated by CMAQ that affects concentration fields. In CMAQ, diffusion processes were treated separately as horizontal diffusion and vertical diffusion. Vertical Diffusion generated by heat, momentum, and moisture fluxes is an important component of vertical transport in the atmosphere (Byun and Ching. 1999). However, large source of uncertainties which either come from lack of fundamental knowledge in vertical diffusion mechanisms, or come from the physical parameterization errors in dry deposition velocity and eddy diffusivity associated with vertical diffusion process could reduce the accuracy of numerical modeling in vertical diffusion of atmospheric properties and chemical species under the convective boundary layer in air quality models (Pleim 2006a, 2006b; Wesely and Hicks, 2000; Wilson 2004).

2.3 Vertical diffusion schemes in CMAQ

Eddy diffusion scheme (EDDY) and the newly developed Asymmetric convective model scheme (ACM2) are two options of vertical diffusion mechanisms in CMAQ to simulate vertical transport of atmospheric properties and chemical species. The EDDY scheme interprets turbulent mixing only in sub-grid-scale (local) considering symmetrical vertical mixing based on concentration gradient between adjacent model layers. The original ACM scheme interprets turbulent mixing only in super-grid-scale (non-local) considering

asymmetrical vertical mixing with fast upward buoyant plume and slow broad compensatory subsidence. The thickness of arrows indicates the quantity of mass flux, reflecting that the mass fluxes increase during the downward transport. The ACM2 scheme combines the above two turbulent mixing schemes enabling the model to simulate vertical transport in both small and large scales. Hence, ACM2 scheme is more realistic in representing vertical mixing process than the other two schemes (Byun and Ching 1999; Pleim 2006). The schematic of three types of vertical transport is shown in Figure 2.3.

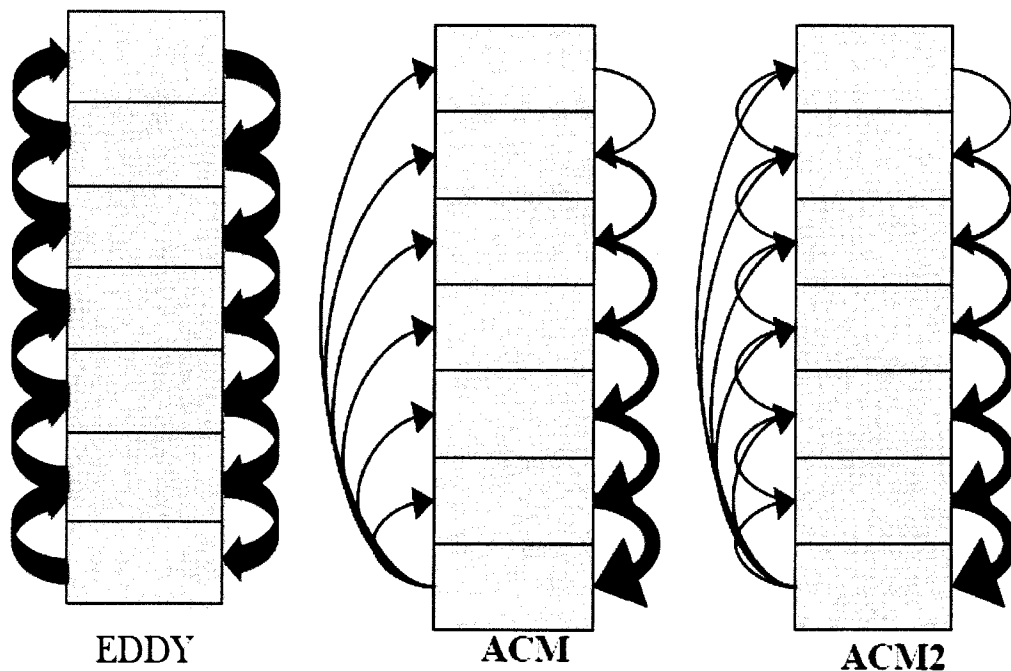


Figure 2.3: Schematic representation of the exchange among model layers in three schemes. (left) EDDY, (middle) ACM, (right) ACM2

The model formulation for EDDY scheme is shown in equation 2.2

$$\frac{\partial C_i}{\partial t} = \frac{1}{\Delta z_i} \left[\frac{K_{i+1/2}(C_{i+1} - C_i)}{\Delta z_{i+1/2}} + \frac{K_{i-1/2}(C_i - C_{i-1})}{\Delta z_{i-1/2}} \right] \quad (2.2)$$

where C_i is the concentration at layer i ; Δz_i is the thickness of layer i ; K is the eddy diffusivity (K_z); i represents the center of the layer; $i+1/2$ represents the layer interface.

In addition to local mixing, the ACM2 scheme also contains a non-local mixing component. The model formulation of ACM2 is shown in equation 2.3 (Pleim 2006a)

$$\begin{aligned} \frac{\partial C_i}{\partial t} = & M2u C_1 - M2d_i C_i + M2d_{i+1} C_{i+1} \frac{\Delta z_{i+1}}{\Delta z_i} \\ & + \frac{1}{\Delta z_i} \left[\frac{K_{i+1/2}(C_{i+1} - C_i)}{\Delta z_{i+1/2}} + \frac{K_{i-1/2}(C_i - C_{i-1})}{\Delta z_{i-1/2}} \right] \end{aligned} \quad (2.3)$$

The first three terms in equation 2.3 represent the asymmetric convective mixing (ACM) as shown in the middle plot of Figure 2.3. The upward and downward mixing rates are shown in equation 2.4a and 2.4b, respectively.

$$M2u = \frac{f_{conv} K_z(z_{1+1/2})}{\Delta z_1 (h - z_{1+1/2})} \quad (2.4a)$$

$$M2d_i = M2u (h - z_{i-1/2}) / \Delta z_i \quad (2.4b)$$

The K used in local mixing (the fourth term in equation 2.3) is different than that used in equation 2.2 and is defined as in equation 2.5. The f_{conv} in the equation 2.4a and 2.5 is a partitioning factor used to control the degree of local and non-local mixing in ACM2 scheme.

$$K(z) = K_z(z)(1 - f_{conv}) \quad (2.5)$$

$$f_{conv} = \left[1 + \frac{k^{-2/3} \left(-\frac{h}{L} \right)^{-1/3}}{0.1a} \right]^{-1} \quad a = 7.2 \quad (2.6)$$

In equation 2.6, k is the von Karman constant ($k = 0.4$), h is PBL height, and L is the Monin-Obukov Length. When $f_{conv} = 1$, the ACM2 scheme converges to original ACM scheme; when $f_{conv} = 0$, the ACM2 will return to EDDY scheme. Under stable or neutral conditions, f_{conv} needs to be zero for pure eddy diffusion.

Using EDDY or ACM2 likely will predict different results in otherwise identical model simulations. Therefore, one type of structural uncertainty will be generated by choosing either EDDY or ACM2 in the model configuration. To quantify this uncertainty, inter-comparisons between modeling results generated from two schemes of a single process and comparison with observed data are required (Pinder et al. 2009). Pleim (2006b; 2009) have conducted a few modeling comparisons between EDDY and ACM2 schemes in the CMAQ model, including modeled ground level ozone concentration from two schemes compared with surface observation data and modeled gas species vertical profiles from two schemes compared with NOAA P-3 aircraft spiral data. The results indicated that the ACM2 scheme tends to predict larger concentrations of secondary pollutants and smaller concentrations of primary pollutants at surface. The ACM2 scheme has a more well-mixed profile under the PBL than the EDDY scheme. However, the differences between simulated results from two schemes are not significant. In order to better quantify these two schemes, more comprehensive evaluations with different scenarios are still highly desirable.

2.4 Vertical eddy diffusivity (K_z)

Vertical eddy diffusivity, K_z , also called vertical eddy diffusion coefficient is used to calculate the diffusion rate in the vertical diffusion process. In the lower troposphere, K_z depends on wind speed, surface roughness, heating of surface, and altitude (Jacob 1999). Many methods have been developed to estimate K_z , but results lack consistency (Wilson 2004). In the CMAQ model, PBL similarity theory is used to parameterize the vertical eddy diffusivity (Byun and Ching, 1999). For the surface layer, the non-dimensional profile functions, ϕ , of the vertical gradient of potential temperature are expressed in equation 2.7 as follows:

$$\phi = \text{Pr}_0(1 + \beta_h z/L) \quad 1 \geq z/L \geq 0 \quad \text{moderately stable} \quad (2.7a)$$

$$\phi = (1 - \gamma_h z/L)^{-1/2} \quad z/L < 0 \quad \text{unstable} \quad (2.7b)$$

$$\phi = \text{Pr}_0(\beta_h + z/L) \quad z/L \geq 1 \quad \text{stable} \quad (2.7c)$$

In equation 2.7, Pr_0 is the Prandtl number of neutral stability, β_h and γ_h are the coefficients of profile functions obtained from field measurements, and L is Monin-Obukhov length.

Parameterization for eddy diffusivity at surface layer is shown in equation 2.8.

$$K_z(z) = \frac{ku_*z}{\phi(z/L)} \quad (2.8)$$

The eddy diffusivity parameterization equation for EDDY and ACM2 schemes are different in the PBL. For the EDDY scheme, the eddy diffusivity is parameterized with the expressions as shown in equation 2.9 (Byun and Ching, 1999)

$$K_z(z) = \frac{ku_*z(1-z/h)^{3/2}}{\phi(z/L)} \quad z/L > 0 \text{ (stable)} \quad (2.9a)$$

$$K_z(z) = kw_*z(1-z/h) \quad z/L < 0 \text{ (unstable)} \quad (2.9b)$$

An integration method was used to parameterize equations 2.8 and 2.9 at model layer interfaces in order to get more accurate results (Byun and Dennis, 1995). For the ACM2 scheme, the parameterization expressions for eddy diffusivity are shown in equation 2.10 based on the Holtslag and Boville method (Pleim 2006a).

$$K_z(z) = k \frac{u_*}{\phi\left(\frac{z_s}{L}\right)} z(1-z/h)^2 \quad z_s = \min(z, 0.1h) \quad z_s/L < 0 \text{ (unstable)} \quad (2.10a)$$

$$K_z(z) = k \frac{u_*}{\phi\left(\frac{z_s}{L}\right)} z(1-z/h)^2 \quad z_s = z \quad z_s/L > 0 \text{ (stable)} \quad (2.10b)$$

In the above equations, u_* is the friction velocity, w_* is the convective velocity, and the values could be obtained by the field measurements. By comparing equation 2.9 and 2.10, we can see that the EDDY scheme uses a quadratic height function to calculate eddy diffusivity and the ACM2 scheme uses a cubic height function. Therefore, EDDY could predict a deeper effective mixing depth than ACM2 (Pleim 2009).

K_z is an empirical quantity. Therefore, uncertainties in eddy diffusivity are unavoidable. Hence, K_z may give parametric uncertainty in the model simulations.

2.5 Dry deposition velocity (V_d)

Dry deposition is the atmospheric process of removing gaseous and particulate species from the atmosphere to the surface of the Earth without precipitation. The dry deposition

rate depends on atmospheric stability, chemical properties of species themselves, and the surface roughness (Seinfeld and Pandis, 2002). The dry deposition flux at some reference height, for example 10m above the surface, can be expressed as an equation shown in 2.11.

$$F = -V_d C \quad (2.11)$$

The process of dry deposition consists three steps: first, aerodynamic transport to a very thin layer called the quasi-laminar sublayer over the surface with stagnant air; second, transport through the quasi-laminar sublayer by molecular diffusion; third, uptake by the Earth surface (Seinfeld and Pandis, 2002). This process is illustrated by analogy to an electrical resistance analogy as shown in Figure 2.4, with three resistances in series

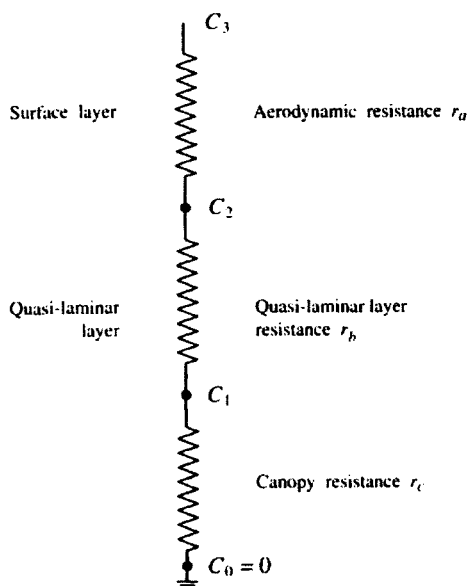


Figure 2.4: Resistance model for dry deposition. (Source: Seinfeld and Pandis, 2002)

In Figure 2.4, aerodynamic resistance, R_a , quasi-laminar layer resistance, R_b , and canopy resistance, R_c are shown. The dry deposition velocity is expressed as the inverse of the sum of the resistances as shown in equation 2.12

$$V_d = (R_a + R_b + R_c)^{-1} \quad (2.12)$$

The dry deposition velocities of chemical species can be modeled by using surface information, surface layer meteorology data, and the dry deposition flux measured in field observations. However, due to the difficulties associated with long-term dry deposition flux measurements in various terrain and the inaccuracies in model inputs, as large as $\pm 30\%$ uncertainty in modeled dry deposition velocity is commonly observed between measured and modeled data (Brook et al., 1999; Wesely and Hicks, 2000). Therefore, the dry deposition velocity may also give parametric uncertainty in the model simulations. A recent uncertainty analysis study conducted by Bergin et al. (1999) indicated that besides the effects of uncertainties in emissions and reaction rate constants of dominant chemical reactions, the effect of uncertainty in ozone dry deposition velocity on ozone concentration simulation is considerable. The uncertainty in NO_2 dry deposition velocity also may have significant impact on simulated HNO_3 formation and responses to NO_x emission reductions.

In CMAQ, dry deposition takes place only at the surface layer. The dry deposition velocities were calculated in MCIP preprocessor and were used by CCTM as inputs.

There are two methods, RADM and M3DDEP, used in MCIP to estimate the dry deposition velocity (Byun and Ching, 1999). RADM was developed by Wesely (1989) and

estimates dry deposition velocity from horizontal wind components, temperature, and humidity profiles (Wesely, 1989). The schematic of pathway resistances used in RADM is shown in Figure 2.5.

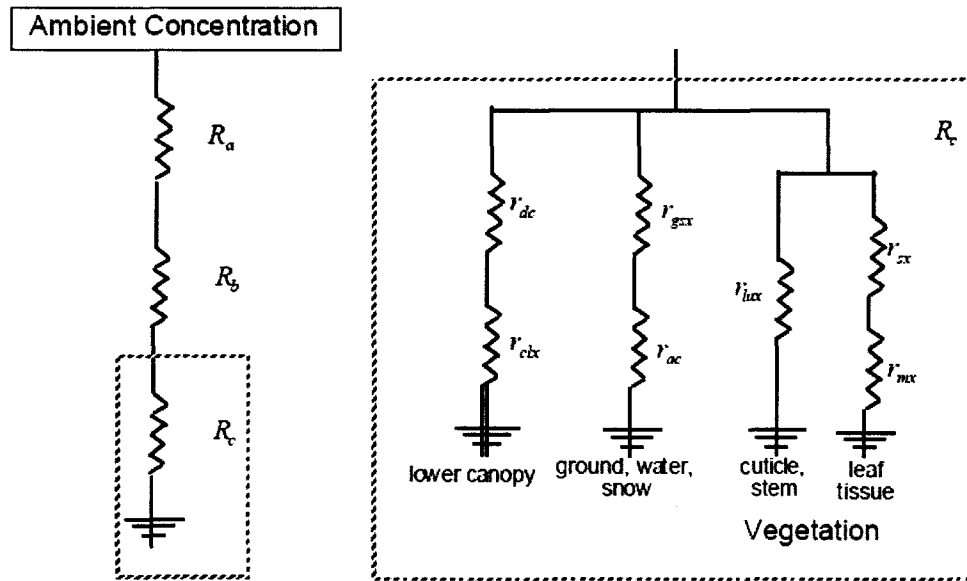


Figure 2.5: Schematic diagram of pathway resistances used in RADM method. (Source: Byun and Ching, 1999)

Resistances R_a , R_b , and R_c in Figure 2.5 are shown in equations 2.13-2.15 (Byun and Ching, 1999).

$$R_a = \int_{z_0}^z \frac{dz}{K_z(z)} = \int_{z_0}^{z_{SL}} \frac{dz}{K_z(z)} + \int_{z_{SL}}^{z_{dep}} \frac{dz}{K_z(z)} = R_{aSL} + R_{aPBL} \quad (2.13)$$

$K_z(z)$ is eddy diffusivity, z_{SL} represents surface layer height, and z_{dep} represents deposition height.

$$R_{hh} = \frac{2}{ku_*} Sc^{2/3} \quad \text{for heat} \quad (2.14a)$$

$$R_{bx} = \frac{2}{ku_*} Sc_x^{2/3} \quad \text{for trace gas species} \quad (2.14b)$$

k is von Karman constant, u_* is friction velocity, and Sc is Schmidt number.

$$R_c = \left(\frac{1}{r_{sx} + r_{mx}} + \frac{1}{r_{lux}} + \frac{1}{r_{dc} + r_{clx}} + \frac{1}{r_{ac} + r_{gsx}} \right) \quad (2.15)$$

In equation 2.15, r_{sx} is the stomatal resistance, r_{mx} is the mesophyl resistance, r_{lux} is the resistance of the outer surface of leaves in the upper canopy, r_{dc} is the resistance for the gas transfer affected by buoyant convection in canopy, r_{clx} the lower canopy resistance, r_{ac} is the resistance that depends on the canopy height, and r_{gsx} is the resistance of soil, leaf litter, and other ground materials.

The M3DDEP method was developed by Pleim (2001), and it uses the same resistance components to estimate the dry deposition velocity but with a new land-surface model (Pleim et al., 2001). The schematic of pathway resistances used in M3DDEP is shown in Figure 2.6.

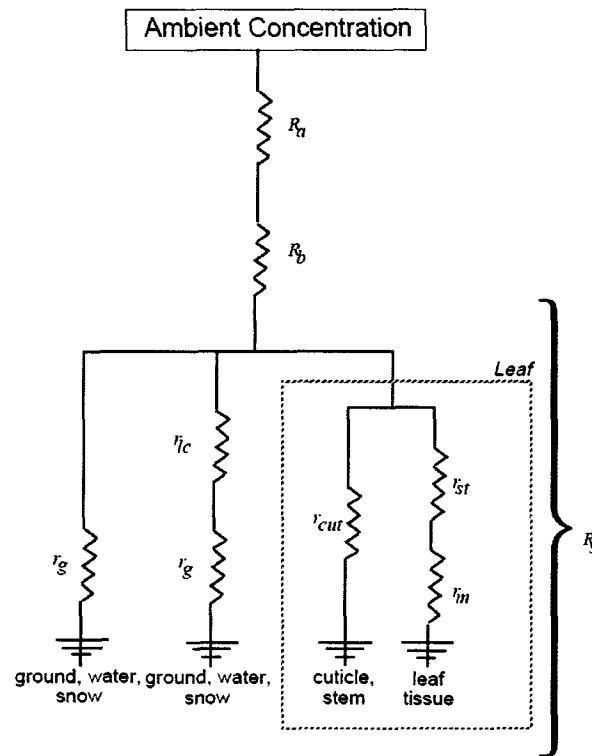


Figure 2.6: Schematic diagram of pathway resistances used in M3DDEP method.

(Source: Byun and Ching, 1999)

In the M3DDEP method, the expression of quasi laminar layer resistances R_b is still the same as equation 2.14; the new expressions for R_a and R_s (surface resistance) are shown in equations 2.16-2.17 (Byun and Ching, 1999).

$$R_a = \rho C_p (\Theta_g - \Theta_1) / H - R_{bh} \quad (2.16a)$$

$$R_a = \frac{Pr_0}{ku_*} \ln \left(\frac{z_1}{z_0} \right) \quad \text{for small sensible heat flux} \quad |H / (\rho C_p)| < 10^{-15} \text{ [K m s}^{-1}] \quad (2.16b)$$

In equation 2.16, Θ_g and Θ_1 are the potential temperature in the air and at the ground surface, respectively in the lowest model layer. z_1 is the height of model layer 1, and z_0 is roughness length.

$$R_s = \left[\frac{f_v}{r_{stb}} + LAI \left(\frac{f_v(1-f_w)}{r_{cut}} + \frac{f_v f_w}{r_{cw}} \right) + \frac{1-f_v}{r_g} + \frac{f_v}{r_{lc} + r_g} \right]^{-1} \quad (2.17)$$

In equation 2.17, r_{stb} is the bulk stomatal resistance including the stomatal resistance on a leaf area r_{st} and the mesophyl resistance r_m as shown in Figure 2.6, r_{cut} is the dry cuticle resistance, r_{cw} is the wet cuticle resistance, r_g is the ground resistance, and r_{lc} is the in-canopy aerodynamic resistance. The vegetation fractional coverage is given by f_v , f_w is the fractional leaf area wetness, and LAI is the leaf area index.

In order to estimate the effects of parametric uncertainties from eddy diffusivity and dry deposition velocity on model performance, sensitivity analysis associated with random sampling technique such as Monte Carlo method could be conducted (Hanna et al., 2001; Pinder et al., 2009). In this study, DDM-3D method was used to calculate the sensitivity coefficients via sensitivity analysis.

2.6 DDM-3D sensitivity analysis

Sensitivity coefficients calculated via sensitivity analysis have been used to determine quantitatively the response of model predictions to variations in the model input and parameters. Numerous methods such as Brute Force, Coupled Direct Method, Green's Function Method (GFM), Automatic Differentiation in Fortran (ADIFOR), and Decoupled Direct Method (DDM) have been developed and used to calculate sensitivity coefficients. Compared to the other methods, sensitivity equations in DDM are derived directly from concentration equations in the base model, and sensitivity coefficients are computed by

DDM at the same time as concentrations. Hence, DDM is more direct, efficient, and stable, and it suffers from less numerical noise than the other methods. It has been used for many years and has been implemented into many models for sensitivity analysis (e.g., Yang et al., 1997; Hakami et al., 2003, 2004).

The methodology for calculation of sensitivity coefficients in DDM is shown below (Hakami et al, 2003).

Equation 2.1 can be rewritten as shown in equation 2.18

$$\frac{\partial C_i}{\partial t} = -\nabla(uC_i) + \nabla(K\nabla C_i) + R_i + E_i \quad (2.18)$$

The initial and boundary conditions used to solve equation 2.18 are shown in equation 2.19 in below.

$$\text{IC: } C_i = C_{0_i} \quad (2.19a)$$

$$\text{BCs: } uC_i - K\nabla C_i = uC_b \quad \text{horizontal inflow} \quad (2.19b)$$

$$-\nabla C_i = 0 \quad \text{horizontal outflow} \quad (2.19c)$$

$$V_{g_i} C_i - K_{zz} \frac{\partial C_i}{\partial z} = E_{0_i} \quad z=0 \quad (2.19d)$$

$$-\frac{\partial C_i}{\partial z} = 0 \quad z=H \text{ (top of model domain)} \quad (2.19d)$$

In equation 2.19, u represents wind field, K represents a second-order turbulent sensor, C_{0_i} and C_b are the initial and boundary concentrations respectively, V_{g_i} is dry deposition velocity, E_{0_i} is ground level emission rate, and i represents species i .

The local sensitivity of a model output to a parameter can be calculated as shown in equation 2.20

$$S_{ij} = \frac{\partial C}{\partial p_j} \quad (2.20)$$

where p_j represents a model parameter. However, due to the variety in magnitudes and units of different parameters, semi-normalized sensitivity coefficients are defined as in equation 2.21

$$S_{ij}^{(1)} = \tilde{p}_j \frac{\partial C_i}{\partial p_j} = \tilde{p}_j \frac{\partial C_i}{\partial(\epsilon_j \tilde{p}_j)} = \frac{\partial C_i}{\partial \epsilon_j} \quad (2.21)$$

where \tilde{p}_j represents a unperturbed field and ϵ_j is a scaling valuable with a nominal value of 1.

Hence, more intuitively, the first order sensitivity coefficients calculations in the expression of differentiating equation 2.1 can be written as in equation 2.22

$$\begin{aligned} \frac{dS_{ij}^1}{dt} = & \frac{\partial}{\partial \epsilon} [advection] + \frac{\partial}{\partial \epsilon} [diffusion] + \frac{\partial}{\partial \epsilon} [deposition] \\ & + \frac{\partial}{\partial \epsilon} [chemistry] + \frac{\partial}{\partial \epsilon} [emission] \end{aligned} \quad (2.22)$$

Meanwhile, equation 2.22 can also be rewritten in the expression of differentiating equation 2.18 as shown in equation 2.23

$$\begin{aligned} \frac{\partial S_{ij}^{(1)}}{\partial t} = & -\nabla(uS_{ij}^{(1)}) + \nabla(K\nabla S_{ij}^{(1)}) + J_i S_j^{(1)} + \frac{\partial R_i}{\partial \epsilon_j} \delta_{5,j_i} + \\ & \tilde{E}_i \delta_{1,j_i} \delta_{j_2} - \nabla(\tilde{u}C_i) \delta_{3,j_i} + \nabla(\tilde{K}\nabla C_i) \delta_{7,j_i} \end{aligned} \quad (2.23)$$

The initial and boundary conditions used to solve equation 2.23 are shown in equation 2.24 in below.

$$\text{IC: } S_{ij}^{(1)} = \tilde{C}_{0,i} \delta_{0,j_i} \delta_{j_2} \quad (2.24a)$$

$$\text{BCs: } uS_{ij}^{(1)} - K\nabla S_{ij}^{(1)} = u\tilde{C}_{b_i} \delta_{2,j_i} \delta_{j_2} + \tilde{u}C_{b_i} \delta_{3,j_i} - \tilde{u}C_i \delta_{3,j_i} + \tilde{K}\nabla C_i \delta_{7,j_i} \quad (2.24b)$$

$$-\nabla S_{ij}^{(1)} = 0 \quad (2.24c)$$

$$v_{g_i} S_{ij}^{(1)} - K_{zz} \frac{\partial S_{ij}^{(1)}}{\partial z} = -\tilde{v}_{g_i} C_i \delta_{6j_1} \delta_{ij_2} + \tilde{K} \frac{\partial C_i}{\partial z} \delta_{7j_1} + \tilde{E}_{0_i} \delta_{1j_1} \delta_{ij_2} \quad (2.24d)$$

$$-\frac{\partial S_{ij}^{(1)}}{\partial z} = 0 \quad (2.24e)$$

In equation 2.23, J_i is the i th row vector in the Jacobian matrix of the reaction rates. δ_{j_1} is the Kronecker delta function used in DDM to control the sensitivity to input parameters that will be calculated during the simulation process. j_1 could be a number from 0 to 6 referring to initial condition, boundary condition, wind field, diffusivity, dry deposition velocity, and reaction rate respectively. δ_{j_2} is used to determine which species will be chosen for sensitivity calculation.

From equation 2.22, we can see that the first order sensitivity considers only the linear model response to input perturbations, as the ‘slope’ shown in Figure 2.7. In order to evaluate the nonlinearity of model response to input perturbations, as the ‘curvature’ shown in Figure 2.7, second order sensitivity coefficients need to be computed.

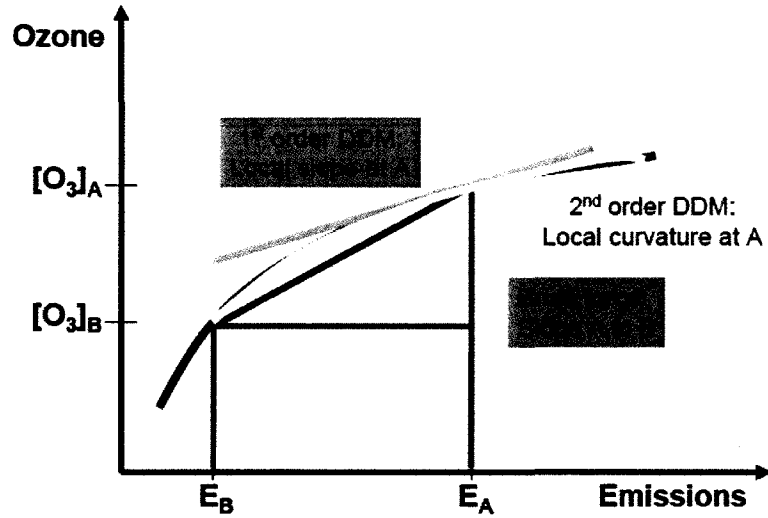


Figure 2.7: Schematic ozone responses to emissions, and brute force and DDM-3D

sensitivities. (Source: Cohan, 2004)

Differentiating equation 2.23 for the same parameter results in the DDM equation for the second order sensitivity coefficients shown in equation 2.25

$$\begin{aligned} \frac{\partial S_{ij}^{(2)}}{\partial t} = & -\nabla(uS_{ij}^{(2)}) + \nabla(K\nabla S_{ij}^{(2)}) + J_i S_j^{(2)} + J_{i,S^{(0)}}^* S_j^{(2)} + \\ & 2 \frac{\partial}{\partial \epsilon_j} (J_{i,\hat{c}} S_j^{(1)}) \delta_{5j_i} - 2\nabla(\tilde{u}S_{ij}^{(1)}) \delta_{3j_i} + \nabla(\tilde{K}\nabla S_{ij}^{(1)}) \delta_{7j_i} \end{aligned} \quad (2.25)$$

The initial and boundary conditions used to solve equation 2.25 are shown in equation 2.26

$$\text{IC: } S_{ij}^{(2)} = 0 \quad (2.26a)$$

$$\text{BCs: } uS_{ij}^{(2)} - K\nabla S_{ij}^{(2)} = -2\tilde{u}S_{ij}^{(1)} \delta_{3j_i} + 2\tilde{K}\nabla S_{ij}^{(1)} \delta_{7j_i} \quad (2.26b)$$

$$-\nabla S_{ij}^{(2)} = 0 \quad (2.26c)$$

$$v_{g_i} S_{ij}^{(2)} - K_{zz} \frac{\partial S_{ij}^{(2)}}{\partial z} = -2\tilde{v}_{g_i} S_{ij}^{(1)} \delta_{6j_i} \delta_{ij_2} + 2\tilde{K} \frac{\partial S_{ij}^{(1)}}{\partial z} \delta_{7j_i} \quad (2.26d)$$

In equation 2.25, $J_{S^{(a)}}^*$ is an augmented Jacobian matrix of reaction rate constants; it has the same structure as $J_{\tilde{c}}$ but without all first order reactions.

The cross sensitivity, second order sensitivity in regards to two different sensitivity parameters, could also be calculated in the same way by differentiating equation 2.23 with respect to a different parameter, but additional terms may be required.

DDM-3D has been implemented into CMAQ successfully for gaseous species by Cohan (2004), and expanded to inorganic particulate matter by Napelenok et al, (2006). CMAQ-DDM can compute the initial condition sensitivity, boundary condition sensitivity, reaction rate constant sensitivity, and emission rate sensitivity. In this study, new features of computing the eddy diffusivity sensitivity and dry deposition velocity sensitivity were also added into CMAQ-DDM. The method of numerical implementation of these two sensitivity parameters in CMAQ-DDM is discussed in chapter 3.

References

- Bergin, M.S., Noblet, G.S., Petrini, K., Dhieux, J.R., Milford, J.B., and Harley, R.B. (1999) Formal uncertainty analysis of a Lagrangian photochemical air pollution model. *Environmental Science and Technology*. 33, 1116-1126.
- Brook, J.R., Zhang, L-M., Di-Giovanni, F., and Padro, J. (1999) Description and evaluation of a model of deposition velocities for routine estimates of air pollutant dry deposition over North America. Part I: model development. *Atmospheric Environment*. 33, 5037-5051.
- Byun, D.W. and Ching, J.K.S. (1999) *Science algorithms of the EPA Model-3 Community Multiscale Air Quality (CMAQ) modeling system*. Office of research and development, US. EPA. North Carolina.
- Byun, D.W. and Dennis, R.L. (1995) Design artifacts in Eulerian air quality models: Evaluation of the effects of layer thickness and vertical profile correction on surface ozone concentrations. *Atmospheric Environment*. 29, 105-126.
- Byun, D.W., Kim, S-T., and Kim, S.B. (2007) Evaluation of air quality models for the simulation of a high ozone episode in the Houston metropolitan area. *Atmospheric Environment*. 41, 837-853.
- Byun, D. and Schere, K.L. (2006) Review of the governing equations, computational algorithms, and other components of the Models-3 Community Multiscale Air Quality (CMAQ) modeling system. *Applied Mechanics Reviews*. 59, 51-77.

CMAS center. *CMAQ v4.6 operational guidance document*.

(http://www.cmaqmodel.org/op_guidance_4.6/index.cfm. Accessed on October 1st, 2009)

Cohan, D.S. (2004) *Photochemical formation and cost-efficient abatement of ozone: high order sensitivity analysis. PhD Dissertation*. The Georgia Institute of Technology, Atlanta, Georgia.

Daum, P.H., Kleinman, L.I., Springston, S.R., Nunnemacker, L.J., Lee, Y-N., Weinstein-Lloyd, J., Zheng, J., and Berkowitz, C. (2004) Origin and properties of plumes of high ozone observed during Texas 2000 Air Quality Study (TEXAQS 2000). *Geophysical Research Letter*. 109, D17306.

Hakami, A., Odman, M.T., and Russell, A.G. (2003) High-order, direct sensitivity analysis of multidimensional air quality models. *Environmental Science and Technology*. 37, 2442-2452.

Hakami, A., Odman, M.T., and Russell, A.G. (2004) Nonlinearity in atmospheric response: A direct sensitivity analysis approach. *Journal of Geophysical Research*. 109, D15303.

Hanna, S.R., Lu, Z., Frey, H.C., Wheeler, N., Vukovich, J., Arumachalam, S., and Fernau, M. (2001) Uncertainties in predicted ozone concentration due to input uncertainties for the UAM-V photochemical grid model applied to the July 1995 OTAG domain. *Atmospheric Environment*. 35, 891-903.

Jacob, D.J. (1999) *Introduction to atmospheric chemistry*. Princeton Press. New Jersey.

- Kleinman, L.I., Daum, P.H., Imre, D., Lee, Y-N., Nunnemacker, L.J., and Springston, S.R. (2002) Ozone production rate and hydrocarbon reactivity in five urban areas: A case of high ozone concentration in Houston. *Geophysical Research Letter*. 29(10), 1467.
- Napelenok, S.L., Cohan, D.S., Hu, Y-T., and Russell, A.G. (2006) Decoupled direct 3D sensitivity analysis for particulate matter (DDM-3D/PM). *Atmospheric Environment*. 40, 6112-6121.
- Parrish, D.D., Allen, D.T., Bates, T.S., Estes, M., Fehsenfeld, F.C., Feingold, G., Ferrare, R., Hardesty, R.M., Meagher, J.F., Nielsen-Gammon, J.W., Pierce, R.B., Ryserson, T.B., Seinfeld, J.H. and Williams, E.J. (2009) Overview of the second Texas Air Quality Study (TexAQS II) and the Gulf of Mexico Atmosphere Composition and Climate Study (GoMACCS). *Journal of Geophysical Research*. 114, D00F13.
- Pinder, R.W., Gilliam, R.C., Appel, K.W., Napelenok, S.L., Foley, K.M., and Gilliland, A.B. (2009) Efficient probabilistic estimates of surface ozone concentration using an ensemble of model configurations and direct sensitivity calculations. *Environmental Science and Technology*. 43, 2388-2393.
- Pleim, J.E. (2006a) A combined local and nonlocal closure model for the atmospheric boundary layer. Part II: Application and evaluation in a mesoscale meteorological model. *Journal of Applied Meteorology and Climatology*. 46, 1396-1408.
- Pleim, J.E. (2006b) A new combined local and non-local PBL model for meteorology and air quality modeling. CMAS conference paper. North Carolina.

Pleim, J.E. Planetary boundary layer modeling for meteorology and air quality.

(http://www.epa.gov/AMD/peer/posters/Poster_1.6.pdf Accessed on September 16th,2009)

Pleim, J.E., Xiu, A., Finkelstein, P.L., and Otte, T.L (2001) A coupled land-surface and dry deposition model and comparison to field measurements of surface heat, moisture, and ozone fluxes. *Water Air Soil Pollution. Focus.* 1, 243-252.

Rappengluck, B., Perna, R., Zhong, S., and Morris, G.A. (2008) An analysis of the vertical structure of the atmosphere and the upper-level meteorology and their impact on surface ozone levels in Houston, Texas. *Journal of Geophysical Research.* 113, D17315.

Ryerson, T.B., et al. (2003) Effect of petrochemical industrial emissions of reactive alkenes and NO_x on tropospheric ozone formation in Houston, Texas. *Journal of Geophysical Research.* 108, D8, 4249.

Seinfeld, J.H and Pandis, S.N (2002) *Atmospheric chemistry and physics.* John Wiley & Sons, INC. New Jersey.

TCEQ. *TexAQS II field study map.*

(http://www.tceq.state.tx.us/implementation/air/airmod/texaqs/texaqs_overview.html Accessed on October 1st, 2009)

Wesely, M.L. (1989) Parameterization of surface resistances to gaseous dry deposition in regional-scale numerical models. *Atmospheric Environment.* 23, 1293-1304.

Wesely, M.L. and Hicks, B.B. (2000) A review of the current status of knowledge on dry deposition. *Atmospheric Environment*. 34, 2261-2282.

Wilson, R. (2004) Turbulent diffusivity in the free atmosphere inferred from MST radar measurements: A review. *Annales Geophysicae*. 22, 3869-3887.

Yang, Y.J., Wilkinson, J.G., and Russell, A.G. (1997) Fast, direct sensitivity analysis of multidimensional photochemical models. *Environmental Science and Technology*. 31, 2859-2868.

CHAPTER 3

Methodology

The methodology of this modeling work is described in this chapter. The following description includes three subsections: Model development, Model evaluation, and Sensitivity and uncertainty analysis. In the model development part, the Crank-Nicolson method that is used to solve the advection-diffusion equation in CMAQ is demonstrated; the numerical implementation of dry deposition velocity and eddy diffusivity sensitivities into the CMAQ-DDM model, and the accuracy test method for the newly implemented code are described. In the model evaluation part, the CMAQ configurations in this study and the data comparison methods are introduced. In the sensitivity and uncertainty analysis part, the sensitivity coefficient calculations and the Taylor expansion equations used in uncertainty analysis are illustrated.

3.1 Model development

3.1.1 Crank-Nicolson scheme

The model formulation of two vertical diffusion schemes, EDDY and ACM2, was described in Chapter Two. To solve the vertical advection-diffusion equation, as shown in equation 3.1, the Crank-Nicolson finite-difference approximation was applied to these two vertical diffusion schemes in CMAQ. Compared to the Forward Euler and Implicit finite-difference methods, which are commonly used in solving differential equations, the

Crank-Nicolson method, as shown in equation 3.2, has second order approximations in both time and space, and it is unconditionally stable for all values of u and K (Jacobson 2005).

$$\frac{\partial N}{\partial t} + \frac{\partial(wN)}{\partial z} - \frac{\partial}{\partial z} \left(K_{zz} \frac{\partial N}{\partial z} \right) = 0 \quad (3.1)$$

$$\begin{aligned} \frac{N_{i,t} - N_{i,t-h}}{h} + \left[\mu_c \frac{(wN)_{i+1,t} - (wN)_{i-1,t}}{2\Delta z} + (1 - \mu_c) \frac{(wN)_{i+1,t-h} - (wN)_{i-1,t-h}}{2\Delta z} \right] \\ - K \left[\mu_c \frac{N_{i+1,t} - 2N_{i,t} + N_{i-1,t}}{\Delta z^2} + (1 - \mu_c) \frac{N_{i+1,t-h} - 2N_{i,t-h} + N_{i-1,t-h}}{\Delta z^2} \right] = 0 \end{aligned} \quad (3.2)$$

In equation 3.2, μ_c is the Crank-Nicolson parameter. When μ_c equals 0, the equation reduces to the forward Euler method; when μ_c equals 1, the equation reduces to the implicit method. In our case, μ_c equals 0.5. The μ_c term enables this method to evaluate some terms at time t and the others at time $t-h$. Hence, it improves the order of approximation in time to second order. The matrix corresponded to equation 3.2 could be written as follows:

$$\begin{aligned} \begin{bmatrix} B_1 & D_1 & 0 & 0 & \dots & 0 & 0 & 0 \\ A_2 & B_2 & D_2 & 0 & \dots & 0 & 0 & 0 \\ 0 & A_3 & B_3 & D_3 & \dots & 0 & 0 & 0 \\ 0 & 0 & A_4 & B_4 & \dots & 0 & 0 & 0 \\ \vdots & \vdots & \vdots & \vdots & & \vdots & \vdots & \vdots \\ 0 & 0 & 0 & 0 & \dots & B_{i-2} & D_{i-2} & 0 \\ 0 & 0 & 0 & 0 & \dots & A_{i-1} & B_{i-1} & D_{i-1} \\ 0 & 0 & 0 & 0 & \dots & 0 & A_i & B_i \end{bmatrix} \begin{bmatrix} N_{1,t} \\ N_{2,t} \\ N_{3,t} \\ N_{4,t} \\ \vdots \\ N_{i-1,t} \\ N_{i-2,t} \\ N_{i,t} \end{bmatrix} = \\ \begin{bmatrix} F_1 & G_1 & 0 & 0 & \dots & 0 & 0 & 0 \\ E_2 & F_2 & G_2 & 0 & \dots & 0 & 0 & 0 \\ 0 & E_3 & F_3 & G_3 & \dots & 0 & 0 & 0 \\ 0 & 0 & E_4 & F_4 & \dots & 0 & 0 & 0 \\ \vdots & \vdots & \vdots & \vdots & & \vdots & \vdots & \vdots \\ 0 & 0 & 0 & 0 & \dots & F_{i-2} & G_{i-2} & 0 \\ 0 & 0 & 0 & 0 & \dots & E_{i-1} & F_{i-1} & G_{i-1} \\ 0 & 0 & 0 & 0 & \dots & 0 & E_i & F_i \end{bmatrix} \begin{bmatrix} N_{1,t-h} \\ N_{2,t-h} \\ N_{3,t-h} \\ N_{4,t-h} \\ \vdots \\ N_{i-1,t-h} \\ N_{i-2,t-h} \\ N_{i,t-h} \end{bmatrix} + \begin{bmatrix} E_1 N_{0,t-h} - A_1 N_{0,t} \\ 0 \\ 0 \\ 0 \\ \vdots \\ 0 \\ 0 \\ G_i N_{i+1,t-h} - D_i N_{i+1,t} \end{bmatrix} \quad (3.3) \\ A_i = -\mu_c h \left(\frac{w}{2\Delta z} + \frac{K_{zz}}{\Delta z^2} \right)_{i-1} \quad B_i = 1 + \mu_c h \left(\frac{2K_{zz}}{\Delta z^2} \right)_i \quad D_i = \mu_c h \left(\frac{w}{2\Delta z} - \frac{K_{zz}}{\Delta z^2} \right)_{i+1} \end{aligned}$$

$$E_i = (1 - \mu_c)h\left(\frac{w}{2\Delta z} + \frac{K_{zz}}{\Delta z^2}\right)_{i-1} \quad F_i = 1 - (1 - \mu_c)h\left(\frac{2K_{zz}}{\Delta z^2}\right)_i \quad G_i = -(1 - \mu_c)h\left(\frac{w}{2\Delta z} - \frac{K_{zz}}{\Delta z^2}\right)_{i+1}$$

Due to the operator splitting method used in the model, the EDDY and ACM2 codes only simulate vertical diffusion, that is, the $K_{zz}/\Delta z^2$ term. The vertical advection term, $w/2\Delta z$, is being simulated by another code called ZADV. Both schemes discretized their diffusion equations into a tridiagonal matrix system, as shown in equation 3.3, and use the Thomas algorithm (tridiagonal solver) to solve the matrix.

3.1.2 Numerical implementation

As described in Chapter Two, the DDM equation for the time evolution of first order sensitivity coefficients is given by equation 3.4 (Hakami et al. 2003)

$$\frac{\partial S_{ij}^{(1)}}{\partial t} = -\nabla(uS_{ij}^{(1)}) + \nabla(K\nabla S_{ij}^{(1)}) + J_i S_j^{(1)} + \frac{\partial R_i}{\partial \epsilon_j} \delta_{5j_1} + \tilde{E}_i \delta_{1j_1} \delta_{ij_2} - \nabla(\tilde{u}C_i) \delta_{3j_1} + \nabla(\tilde{K}\nabla C_i) \delta_{7j_1} \quad (3.4)$$

Equation 3.5 is one of the boundary conditions required to solve the first order sensitivity coefficients, and it is also the equation used to calculate the sensitivity to emission, dry deposition velocity, and eddy diffusivity.

$$v_{g_i} S_{ij}^{(1)} - K_{zz} \frac{\partial S_{ij}^{(1)}}{\partial z} = -\tilde{v}_{g_i} C_i \delta_{6j_1} \delta_{ij_2} + \tilde{K}_{zz} \frac{\partial C_i}{\partial z} \delta_{7j_1} + \tilde{E}_{0_i} \delta_{1j_1} \delta_{ij_2} \quad (3.5)$$

V_g , K_{zz} and E represent the dry deposition velocity, eddy diffusivity and emission, respectively. The Kronecker delta function, δ_{j_1} , is used in DDM to control the sensitivity to input parameters that will be calculated during the simulation process. In this work, $6j_1$ and $7j_1$ refer to dry deposition velocity and eddy diffusivity, respectively. δ_{j_2} is used to

determine which species will be chosen for sensitivity calculation. The dry deposition velocities, like emission rates, have different values for different species; hence, the term δ_{j2} needs to be applied to the dry deposition velocity sensitivity calculation. However, δ_{j2} is not necessary for calculating the eddy diffusivity sensitivity because eddy diffusivity does not depend on the properties of species. The DDM code for calculating the emission, dry deposition velocity, and eddy diffusivity sensitivities in equation 3.5 can be implemented into the code that is used to simulate the vertical diffusion process in CMAQ by following the logic of calculating concentrations. The DDM code already has been implemented into the EDDY scheme for emission sensitivity calculation only, but it has not been implemented yet into the newly developed ACM2 scheme. Hence, by analogy to the DDM implementation in the EDDY scheme, the DDM also could be added to the ACM2 scheme. Meanwhile, the first order sensitivities to dry deposition velocity and eddy diffusivity also could be added to the CMAQ-DDM model similarly.

In equation 3.5, for the first order sensitivity, there are three terms on the right hand side. The E_i term already has been added to DDM in the EDDY scheme as mentioned above. Hence, by following the same logic, the other two terms, $\tilde{v}_{g_i} C_i \delta_{6j_1} \delta_{ij_2}$ and $\tilde{K} \frac{\partial C_i}{\partial z} \delta_{4j_1}$, are included directly after the E_i term in the code. The capability of calculating dry deposition velocity sensitivity for different species at a particular time and in a given region and the capability of calculating eddy diffusivity sensitivity for different layers at a particular time and in a given region were also added to the DDM code.

After differentiating equation 3.4 for the same parameter, the DDM equation for the

second order sensitivity coefficients is shown in equation 3.6

$$\begin{aligned} \frac{\partial S_{ij}^{(2)}}{\partial t} = & -\nabla(uS_{ij}^{(2)}) + \nabla(K\nabla S_{ij}^{(2)}) + J_i S_j^{(2)} + J_{i,S^{(1)}}^* S_j^{(2)} + \\ & 2 \frac{\partial}{\partial \epsilon_j} (J_{i,c} S_j^{(1)}) \delta_{5j_1} - 2\nabla(\tilde{u}S_{ij}^{(1)}) \delta_{3j_1} + \nabla(\tilde{K}\nabla S_{ij}^{(1)}) \delta_{7j_1} \end{aligned} \quad (3.6)$$

Equation 3.7, as one of the boundary condition for 3.6, can be used as guidance for the implementation of the second order sensitivities to dry deposition velocity and eddy diffusivity.

$$v_{g_i} S_{ij}^{(2)} - K_{zz} \frac{\partial S_{ij}^{(2)}}{\partial z} = -2\tilde{v}_{g_i} S_{ij}^{(1)} \delta_{6j_1} \delta_{ij_2} + 2\tilde{K}_{zz} \frac{\partial S_{ij}^{(1)}}{\partial z} \delta_{7j_1} \quad (3.7)$$

The emission term in equation 3.5 does not appear in equation 3.7, because it has concentration term (C_i) for dry deposition and eddy diffusion in the first order sensitivity calculation, the additional terms with first order sensitivities appear in equation 3.7 for second order sensitivities to dry deposition velocity and eddy diffusivity calculation. Similarly, second order terms also could be added into DDM by following the same protocol that has been used in the first order sensitivity implementation.

For the second order sensitivity, two additional terms were required for HDDM,

$$-2\tilde{v}_{g_i} S_{ij}^{(1)} \delta_{6j_1} \delta_{ij_2} \text{ and } 2\tilde{K}_{zz} \frac{\partial S_{ij}^{(1)}}{\partial z} \delta_{4j_1},$$

as shown on the right hand side of equation 3.7. The implementation of second order terms is very similar to that for the first order terms. The only difference is that the concentration terms in first order sensitivities calculations were replaced by the corresponding first order sensitivity terms. Notice that the logic in equation 3.7 is only for the same sensitivity parameter. For second order of different sensitivity parameters, such as cross sensitivity of dry deposition with emission, the term on the right

hand side of equation 3.7 should be replaced by $-\tilde{v}_g \delta_{6j_1} \delta_{ij_2} S_{ik}^{(1)}$, where $S_{ik}^{(1)}$ indicates the other sensitivity parameter, here referring to emission.

For the DDM implementation of the first order and second order sensitivities to dry deposition velocity and eddy diffusivity, the logic and the way of coding are almost identical for the EDDY and ACM2 schemes. The only difference is that the non-local turbulence diffusion terms under the convective boundary layer also need to be considered in the DDM for eddy diffusivity sensitivity calculation for the ACM2 scheme.

3.1.3 Accuracy test

After new code is implemented into DDM, an accuracy test is essential for model validation. Commonly, the sensitivity coefficients calculated by DDM are compared with a Brute Force approximation to evaluate the accuracy (Hakami et al., 2004). Sensitivity coefficients calculated by a Brute Force approximation are derived from Taylor series expansion and are shown in equations 3.8-3.10. Equation 3.8 can be used for first order sensitivity comparison, equation 3.9 can be used for second order sensitivity comparison, and equation 3.10 can be used for cross sensitivity comparison

$$S_j^{(1)} \approx \frac{C_{+\Delta\epsilon_j} - C_{-\Delta\epsilon_j}}{2\Delta\epsilon_j} \quad (3.8)$$

$$S_{j,j}^{(2)} \approx \frac{C_{(+\Delta\epsilon_j, p_j)} - 2C_0 + C_{(-\Delta\epsilon_j, p_j)}}{(\Delta\epsilon_j)^2} \quad (3.9)$$

$$S_{j,k}^{(2)} \approx \frac{C_{(+\Delta\epsilon_j, p_j, +\Delta\epsilon_k, p_k)} - C_{(+\Delta\epsilon_j, p_j, -\Delta\epsilon_k, p_k)} - C_{(-\Delta\epsilon_j, p_j, +\Delta\epsilon_k, p_k)} + C_{(-\Delta\epsilon_j, p_j, -\Delta\epsilon_k, p_k)}}{4\Delta\epsilon_j \Delta\epsilon_k} \quad (3.10)$$

$\Delta \in$ in above equations indicates the perturbation of model input parameters in the Brute Force approximation. In this study, $\pm 10\%$ perturbation was chosen for the first order sensitivity coefficients calculation by the Brute Force approximation, and $\pm 50\%$ perturbation was chosen for the second order and cross sensitivity coefficients calculation.

3.2 Model evaluation

3.2.1 Model configurations

CMAQ model version 4.5 was used in this study to simulate a seven-day episode from August 30th to September 5th in eastern Texas at a resolution of 4km grid cell. All model inputs were provided by University of Houston. The model configurations are shown in Figure 3.1 (University of Houston IMAQS. 2009):

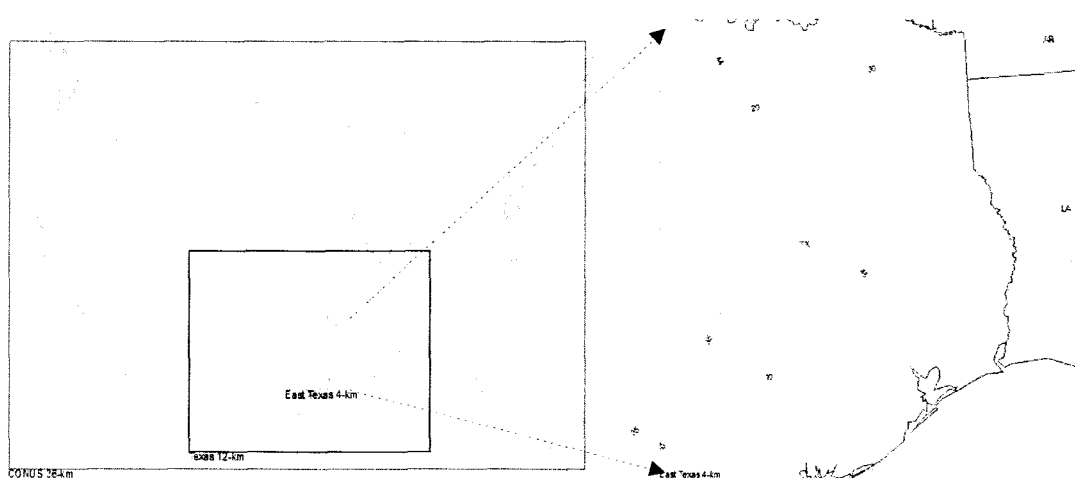


Figure 3.1: Modeling domain of East Texas (source: IMAQS 2009)

The NCAR/Penn State (National Center for Atmospheric Research/Pennsylvania State University) Mesoscale Model, Version 5, release 3.6.1 (MM5V3.6.1), was used to generate the meteorological field in this study, and a 43-layer vertical structure was set up in MM5. The Meteorology-Chemistry Interface Processor Version 2.3 (MCIP2.3) was used to create CMAQ-ready meteorology data from the files generated by MM5, and the 43 vertical layers used in MM5 were reduced to 23 for CMAQ by MCIP. The Sparse Matrix Operator Kernel Emissions (SMOKE) model, version 2.1 was used for emission processing as shown in Figure 3.2. The projected air quality forecast emissions inventory including Point, Mobile, and Area sources at level of year 2005 based on year 2000 and 2007 emissions from TCEQ was used in this study. The biogenic emission inventory is taken from TCEQ's Land Use and Land Cover (LULC) data after processed by the GloBEIS 3.1 model for emission normalizing and by BEIS3 model for meteorology conditions adjustment.

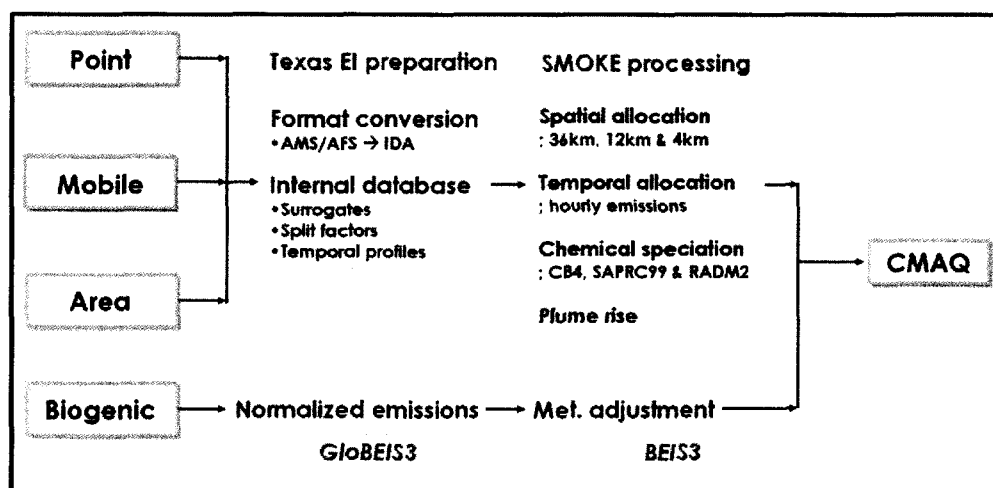


Figure 3.2: SMOKE emissions processing (source: IMAQS 2009)

The CMAQ model configuration is shown in Table 3.1.

Table 3.1: CMAQ science options (source: IMAQS 2009)

Options	Parameters
Domain	Eastern Texas 4-km
CMAQ	Version 4.5
MCIP	Version 2.3
SMOKE	Version 2.1
Chemical Mechanism	CB4 (cb4_aq_ae4)
Emissions	Texas Emissions Inventory (TCEQ) projected for 2005 + NEI99
Boundary Condition	Downscale linkage from GEOS-CHEM
Advection Scheme	Piecewise Parabolic Method (PPM)
Horizontal Diffusion	Multiscale
Vertical Diffusion	Eddy
Cloud Scheme	RADM
Forecasting hours	48 hours (+ 6-hr spin-up)

3.2.2 Data comparisons

In this study, the modeling results generated by using different vertical diffusion schemes, EDDY and ACM2, were compared with the field measurement data from a TexAQs 2006/Gulf of Mexico Atmospheric Composition and Climate Study (GoMACCS)

Comparisons in this study include those with surface data, ozonesonde data, and aircraft data. As shown in Figure 3.3, the red rectangle represents ground site measurements, and the data were downloaded from TECQ website (http://www.tceq.state.tx.us/compliance/monitoring/air/monops/hourly_data.html). The green circle and blue ship sign represent the ozonesonde measurements conducted at University of Houston and the Houston Ship Channel, respectively, and the data were downloaded from World Ozone Data Centre website (<ftp://ftp.tor.ec.gc.ca/Projects-Campaigns/ions06/>). The air plane sign represents NOAA P-3 Aircraft measurements, and the data were downloaded from NOAA website (<http://www.esrl.noaa.gov/csd/tropchem/2006TexAQS/>).

The measurement data were compared to the modeling results from CMAQ extracted from output netCDF files for the corresponding grid cell, hour, and layer.

3.3 Sensitivity and Uncertainty analysis

In this study, the sensitivity analysis and the uncertainty analysis in dry deposition velocity for both EDDY and ACM2 schemes were investigated. However, the uncertainty analysis in eddy diffusivity was not performed, because K_z is a meteorological parameter, and if only considers the variation in CMAQ alone, it may cause model inconsistency error between MM5 and CMAQ.

3.3.1 Sensitivity analysis

As described in Chapter Two, the semi-normalized first order sensitivity coefficients can be written as equation 3.11. Similarly, the semi-normalized second order sensitivity coefficients for the same and different parameters can be also defined as equation 3.12 and 3.13, respectively.

$$S_j^{(1)} = P_j \frac{\partial C}{\partial p_j} = P_j \frac{\partial C}{\partial(\epsilon_j P_j)} = \frac{\partial C}{\partial \epsilon_j} \quad (3.11)$$

$$S_{j,j}^{(2)} = P_j \frac{\partial}{\partial p_j} \left(P_j \frac{\partial C}{\partial p_j} \right) = \frac{\partial^2 C}{\partial \epsilon_j^2} \quad (3.12)$$

$$S_{j,k}^{(2)} = P_j \frac{\partial}{\partial p_j} \left(P_k \frac{\partial C}{\partial p_k} \right) = \frac{\partial^2 C}{\partial \epsilon_j \partial \epsilon_k} \quad (3.13)$$

The P_j and P_k in above equations represent the input or model parameters such as emission rate, dry deposition velocity, or boundary condition. The p_j and p_k represent the variations of model parameters such as P_j and P_k , and are defined as $p = \epsilon P$. ϵ is a scaling variable with nominal value 0 to 1.

The first order sensitivity coefficients evaluate the responsiveness of pollutant concentration to infinitesimal perturbations of model parameters; the second order sensitivity coefficients quantify the nonlinearity of the pollutant concentration response; the cross sensitivity coefficients analyze the effectiveness of pollutant concentration response to one sensitivity parameter influenced by the other sensitivity parameter (Cohan et al., 2005). In this study, the first order and second order ozone sensitivities to anthropogenic NO_x emission, to anthropogenic VOC emission and to dry deposition

velocity of all species were analyzed.

By looking at the first order ozone sensitivities to anthropogenic NO_x , $\partial[O_3]/\partial \in_{E,NO_x}$, and to anthropogenic VOC, $\partial[O_3]/\partial \in_{E,VOC}$, the different emission control beneficial regions could be determined for policy applications. For example, where $\partial[O_3]/\partial \in_{E,NO_x} < 0$, controlling VOC will be effective for ozone reduction; where $\partial[O_3]/\partial \in_{E,NO_x} > \partial[O_3]/\partial \in_{E,VOC} > 0$, controlling NO_x will be effective for ozone reduction; where $\partial[O_3]/\partial \in_{E,VOC} > \partial[O_3]/\partial \in_{E,NO_x} > 0$, controlling VOC will be more beneficial than controlling NO_x for ozone reduction (Jin et al., 2008).

By looking at the second order ozone sensitivities to NO_x , $\partial^2[O_3]/\partial \in_{E,NO_x}^2$, to VOC, $\partial^2[O_3]/\partial \in_{E,VOC}^2$, and to dry deposition velocity, $\partial^2[O_3]/\partial \in_{V,dep}^2$, the nonlinear response in ozone concentration to these sensitivity parameters can be quantified. By looking at the cross sensitivity of ozone to emission crossed with dry deposition velocity, $\partial(\frac{\partial[O_3]}{\partial \in_E})/\partial \in_{V,dep}$, the effect of variation in dry deposition velocity on emission control can be evaluated.

3.3.2 Uncertainty in dry deposition velocity

Based on the sensitivity coefficients calculated by DDM, the pollutant concentration with any fractional perturbation can be projected from the base case scenario via Taylor expansion (Hakami et al., 2004; Cohan et al., 2005). The expression of Taylor expansion in this study can be written as equation 3.14

$$C_j |_{p_j=p_j+\Delta \in_j} \approx C_0 |_{p_j=p_j} + \Delta \in_j S_j^{(1)} + \frac{1}{2} \Delta \in_j^2 S_j^{(2)} \quad (3.14)$$

Hence, the effect of uncertainty in dry deposition velocity on model simulation results can be evaluated via Taylor expansion. In this analysis, equation 3.14 was revised and expressed as shown in equation 3.15.

$$C_{\Delta V_{dep}} \approx C_0 + \Delta\phi_{V_{dep}} \times S_{V_{dep}}^{(1)} \quad (3.15)$$

$C_{\Delta V_{dep}}$ in equation 3.15 is the adjusted concentration by considering the effect of uncertainty in dry deposition velocity. $\Delta\phi$ represents uncertainty in dry deposition velocity, a value of $\pm 30\%$ (Wesely and Hicks 2000) will be used in this study.

In addition, the effect of uncertainty in dry deposition velocity on emission control strategies also can be quantified via Taylor series expansion.

$$C(x_0 + \Delta\varepsilon_1, y_0 + \Delta\varepsilon_2) \approx C(x_0, y_0) + \Delta\varepsilon_1 S_{\varepsilon_1}^{(1)}(x_0, y_0) + \frac{(\Delta\varepsilon_1)^2}{2} S_{\varepsilon_1}^{(2)}(x_0, y_0) \quad (3.16)$$

In equation 3.16, x_0 can be considered as emission rate, y_0 can be considered as dry deposition velocity, $\Delta\varepsilon_1$ can be considered as control percentage in emission, and $\Delta\varepsilon_2$ can be considered as uncertainty in dry deposition velocity. In equation 3.16, $\Delta\varepsilon_2$ equals to 0. However, if the parameter y_0 varies ($\Delta\varepsilon_2 > 0$), then more terms must be accounted for equation 3.16 as shown in equation 3.17.

$$C(x_0 + \Delta\varepsilon_1, y_0 + \Delta\varepsilon_2) \approx C(x_0, y_0) + \Delta\varepsilon_1 S_{\varepsilon_1}^{(1)}(x_0, y_0) + \Delta\varepsilon_2 S_{\varepsilon_2}^{(1)}(x_0, y_0) + \frac{(\Delta\varepsilon_1)^2}{2} S_{\varepsilon_1}^{(2)}(x_0, y_0) + \frac{(\Delta\varepsilon_2)^2}{2} S_{\varepsilon_2}^{(2)}(x_0, y_0) + (\Delta\varepsilon_1)(\Delta\varepsilon_2) S_{\varepsilon_1 \varepsilon_2}^{(2)}(x_0, y_0) \quad (3.17)$$

In order to make the left hand side of equation 3.16 equals to that of equation 3.17, the term, $S_{\varepsilon_1}^{(1)}(x_0, y_0)$, in equation 3.16 needs to be updated to the term as in equation 3.18

$$S_{\varepsilon_1}^{(1)}(x_0, y_0) = S_{\varepsilon_1}^{(1)}(x_0, y_0) + \Delta\varepsilon_2 S_{\varepsilon_1 \varepsilon_2}^{(2)}(x_0, y_0) \quad (3.18)$$

Therefore, analog to equation 3.18, we could get the mathematical expressions for quantifying the effect of uncertainty in dry deposition velocity on NO_x and VOC controls as shown in equations 3.19 and 3.20, respectively.

$$S_{E_{\text{NO}_x}}^{(1)} = \left(\frac{\partial[\text{O}_3]}{\partial \epsilon_{E_{\text{NO}_x}}} \right)_{\text{new}} = \left(\frac{\partial[\text{O}_3]}{\partial \epsilon_{E_{\text{NO}_x}}} \right)_{\text{old}} + \Delta \phi_{V_{\text{dep}}} \frac{\partial^2[\text{O}_3]}{\partial \epsilon_{E_{\text{NO}_x}} \partial \epsilon_{V_{\text{dep}}}} \quad (3.19)$$

$$S_{E_{\text{VOC}}}^{(1)} = \left(\frac{\partial[\text{O}_3]}{\partial \epsilon_{E_{\text{VOC}}}} \right)_{\text{new}} = \left(\frac{\partial[\text{O}_3]}{\partial \epsilon_{E_{\text{VOC}}}} \right)_{\text{old}} + \Delta \phi_{V_{\text{dep}}} \frac{\partial^2[\text{O}_3]}{\partial \epsilon_{E_{\text{VOC}}} \partial \epsilon_{V_{\text{dep}}}} \quad (3.20)$$

References

- Cohan D.S., Hakami, A., Hu, Y.T., and Russell, A.G. (2005) Nonlinear response of ozone to emissions: Source apportionment and sensitivity analysis. *Environmental Science and Technology*. 39, 6739-6748.
- Hakami, A., Odman, M.T., and Russell, A.G. (2003) High-order, direct sensitivity analysis of multidimensional air quality models. *Environmental Science and Technology*. 37, 2442-2452.
- Hakami, A., Odman, M.T., and Russell, A.G. (2004) Nonlinearity in atmospheric response: A direct sensitivity analysis approach. *Journal of Geophysical Research*. 109, D15303.
- Jacobson, M.Z. (2005) *Fundamentals of Atmospheric Modeling*. Cambridge University Press, New York.
- Jin, L., Tonse, S., Cohan, D.S., Mao, X.L., Harley, R.A., and Brown, N.J. (2008) Sensitivity analysis of ozone formation and transport for a central California air pollution episode. *Environmental Science and Technology*. 42, 3683-3689.
- UH IMAQS. *Air Quality Forecasting Model Configurations*.
(<http://imaqs.uh.edu/ModelSetup.html>. Accessed on October 15th, 2009)
- Wesely, M.L. and Hicks, B.B. (2000) A review of the current status of knowledge on dry deposition. *Atmospheric Environment*. 34, 2261-2282.

CHAPTER 4

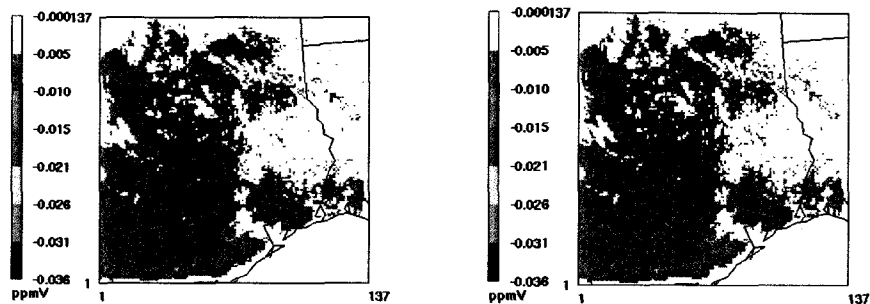
Results and Discussions

In this chapter, modeling results will be illustrated and discussed. It includes four parts: accuracy test, vertical diffusion scheme evaluation, sensitivity analysis, and effect of uncertainty in dry deposition velocity.

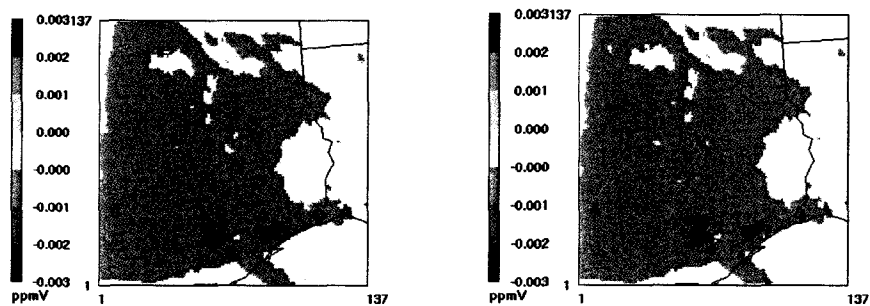
4.1 Accuracy test results

As described in Chapter Three, sensitivity coefficients calculated by a Brute Force approximation are used as a benchmark of DDM accuracy. The equations for sensitivity coefficients calculation from the Brute Force approximation are shown in equation 3.8-3.10 in Chapter Three. The comparisons of sensitivity coefficient calculation between DDM and the Brute Force approximation approach are presented in this section. The first order sensitivity coefficients of ozone to ozone dry deposition velocity, ozone to eddy diffusivity, and ozone to NO_x dry deposition velocity, the second order sensitivity coefficient of ozone to NO_x dry deposition velocity, and the cross sensitivity coefficient between NO_x dry deposition velocity and NO_x emission are tested for both EDDY (Figure 4.1a) and ACM2 (Figure 4.1b) schemes.

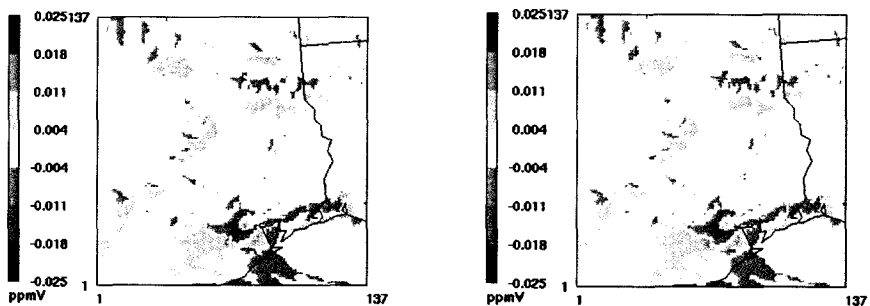
$\partial[O_3]/\partial \epsilon_{V_{O_3,dep}}$ (ozone sensitivity to ozone dry deposition velocity)



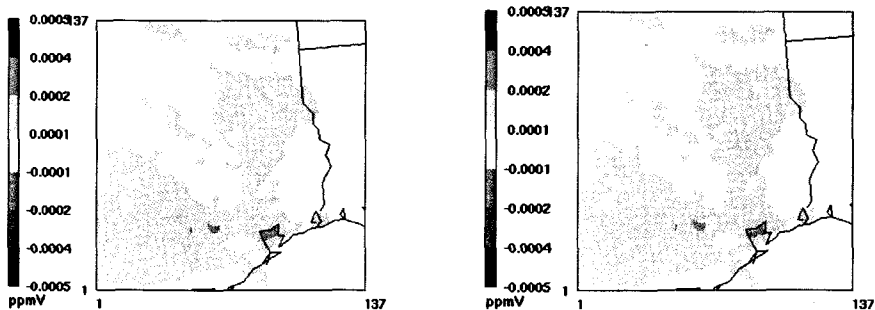
$\partial[O_3]/\partial \epsilon_{V_{NO_x,dep}}$ (ozone sensitivity to NO_x dry deposition velocity)



$\partial[O_3]/\partial \epsilon_{K_{zz}}$ (ozone sensitivity to eddy diffusivity)



$\partial^2[O_3]/\partial \epsilon_{V_{NO_x,dep}}^2$ (second order ozone sensitivity to NO_x dry deposition velocity)



$$\partial^2[O_3]/\partial \epsilon_{E_{NO_x}} \partial \epsilon_{V_{NO_x,dep}} \quad (\text{cross sensitivity to } NO_x \text{ emission and } NO_x \text{ dry deposition velocity})$$

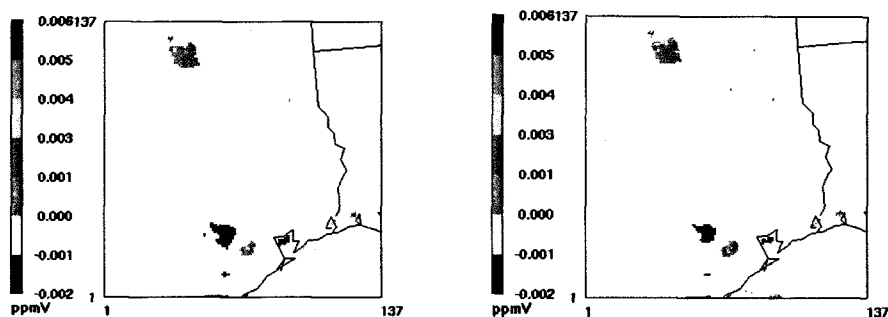
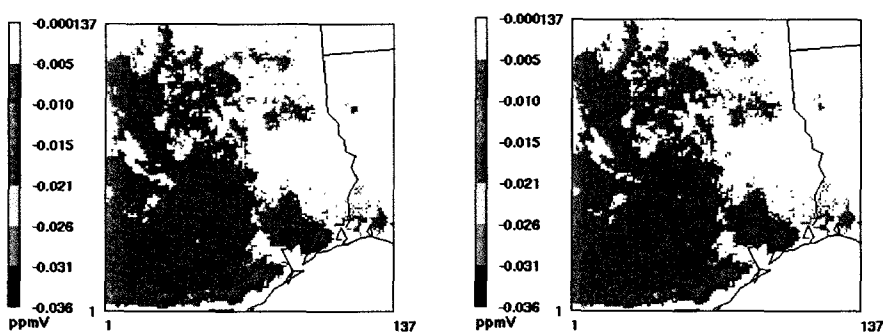
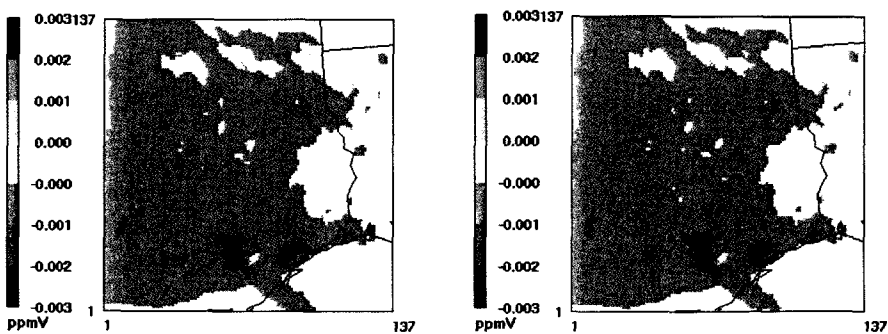


Figure 4.1a: Sensitivity coefficients from DDM (left) and Brute Force (right) of EDDY scheme at the time of peak ozone (4:00PM CST) on August 31st, 2006.

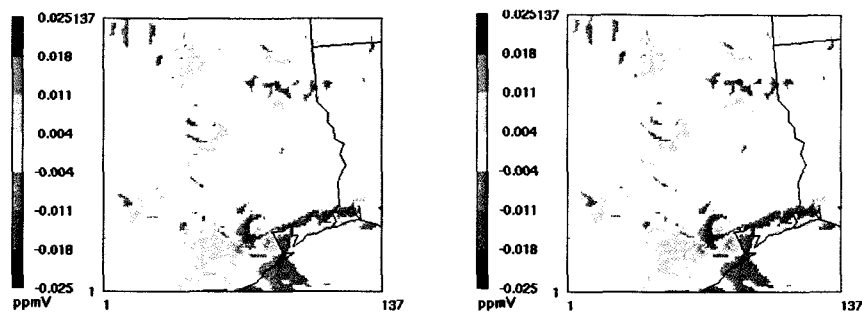
$$\partial[O_3]/\partial \epsilon_{V_{O_3,dep}} \quad (\text{ozone sensitivity to ozone dry deposition velocity})$$



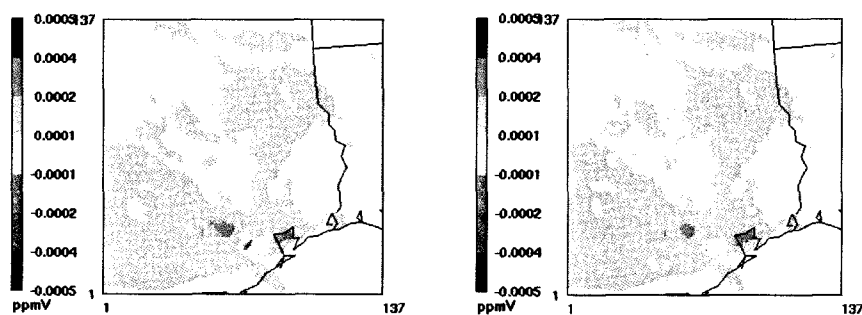
$$\partial[O_3]/\partial \epsilon_{V_{NO_x,dep}} \quad (\text{ozone sensitivity to } NO_x \text{ dry deposition velocity})$$



$\partial[O_3]/\partial \epsilon_{K_{zz}}$ (ozone sensitivity to eddy diffusivity)



$\partial^2[O_3]/\partial \epsilon_{V_{NO_x,dep}}^2$ (second order ozone sensitivity to NO_x dry deposition velocity)



$\partial^2[O_3]/\partial \epsilon_{E_{NO_x}} \partial \epsilon_{V_{NO_x,dep}}$ (cross sensitivity to NO_x emission and NO_x dry deposition velocity)

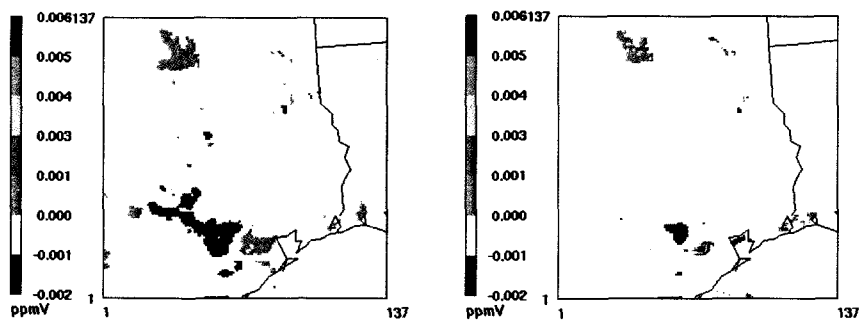


Figure 4.1b: Sensitivity coefficients from DDM (left) and Brute Force (right) of ACM2 scheme at the time of peak ozone (4:00PM CST) on August 31st, 2006.

Table 4.1. Sensitivity coefficients of 1-hour ozone with respect to dry deposition velocity, eddy diffusivity, and emission, and statistical consistency of Brute Force and DDM-3D results

Sensitivity Parameters	DDM vs. Brute Force (EDDY) ^a			DDM vs. Brute Force (ACM2) ^a		
	R ²	Bias% ^f	Error% ^g	R ²	Bias% ^f	Error% ^g
O ₃ dry deposition velocity ^{b,c}	0.9991	-0.19	0.94	0.9989	-0.72	1.2
NO _X dry deposition velocity ^{b,d}	0.9953	2.17	3.02	0.9955	2.04	3.05
Eddy diffusivity ^{b,e}	0.9932	-1.72	3.91	0.9911	3.3	5.91
1 st order domain wide NO _X emission ^b	0.9975	-1.60	3.22	0.9975	-1.39	3.1
2 nd order dry deposition velocity ^{d,h}	0.9595	0.59	6.77	0.9046	10.58	17.99
Cross sensitivity (E _{NOX} and V _{dNOX}) ⁱ	0.9676	16.64	13.74	0.845	21.25	33.1

Note: a Comparing for each day and grid cell. Averaged over domain for Aug. 31-Sep 5 episode.

b Calculated using $\pm 10\%$ perturbation

c O₃ sensitivity to O₃ dry deposition velocity

d O₃ sensitivity to NO_X dry deposition velocity

e O₃ sensitivity to eddy diffusivity in all layers

f Normalized mean bias $\Sigma(\text{DDM}-\text{Brute force})/\Sigma(\text{Brute force})$

g Normalized mean error $\Sigma|(\text{DDM}-\text{Brute force})|/\Sigma|(\text{Brute force})|$

h Calculated using $\pm 50\%$ perturbation

i Calculated using $\pm 10\%$ perturbation for emission, $\pm 50\%$ perturbation for dry deposition velocity

The first order sensitivity coefficients calculated by DDM and the Brute Force method are almost identical for both schemes. The second order sensitivity and cross sensitivity coefficients calculated by DDM seem to be less accurate but still have good agreement compared with Brute Force (Figure 4.1). The statistical analysis results (Table 4.1) show the same conclusions as those illustrated in Figure 4.1. The statistical comparisons between DDM and BF in Table 4.1 were calculated cell-by-cell for each hour in a day and were averaged over six days of the episode. A $\pm 50\%$ perturbation was used in the Brute Force approximation for second order sensitivity to dry deposition velocity in order to reduce the

numerical noise from model simulations. The first day statistical results were excluded in the calculations to minimize influence of the initial conditions. The statistical results show R^2 close to one and very small values of normalized mean bias (NMB) and normalized mean error (NME) for the first order sensitivity coefficients comparisons. However, the second order and cross sensitivity coefficients have slightly less statistical consistency than the first order coefficients, most probably due to truncation error and model inconsistency error from the Brute Force approximation (Hakami et al., 2004). Notice that the second order and cross sensitivity coefficients from ACM2 scheme showed remarkable inaccuracy. Hence, the HDDM code for the second order and cross sensitivity of dry deposition velocity in ACM2 requires further investigation. Additionally, weak consistency was observed in modeling cases with a grid size larger than 8km because of the convective cloud process during the simulation. Scientists at U.S. EPA are addressing this weakness (Sergey, N.L, personal communications, 2009).

4.2 Vertical diffusion schemes evaluation

The CMAQ model simulation results with two different vertical diffusion schemes for the same episode are evaluated in this section. The data comparisons between modeling and measurements include those with surface, ozonesonde, and regional aircraft data.

4.2.1 Regional ozone modeling

Ozone formation and transport in eastern Texas from August 30th to September 5th were simulated by CMAQ 4.5. The maximum 1-hr average simulated ozone in the episode occurs downwind of the Houston Ship Channel at 4:00PM (CST) on August 31st, 2006, and the predicted ozone concentration reaches 133ppb in EDDY scheme and 147 ppb in ACM2 scheme. The eastern Texas county map and HGB ozone non-attainment area are shown in Figure 4.2. The wind conditions and PBL height over the study domain at the time of peak ozone are shown in Figure 4.3.

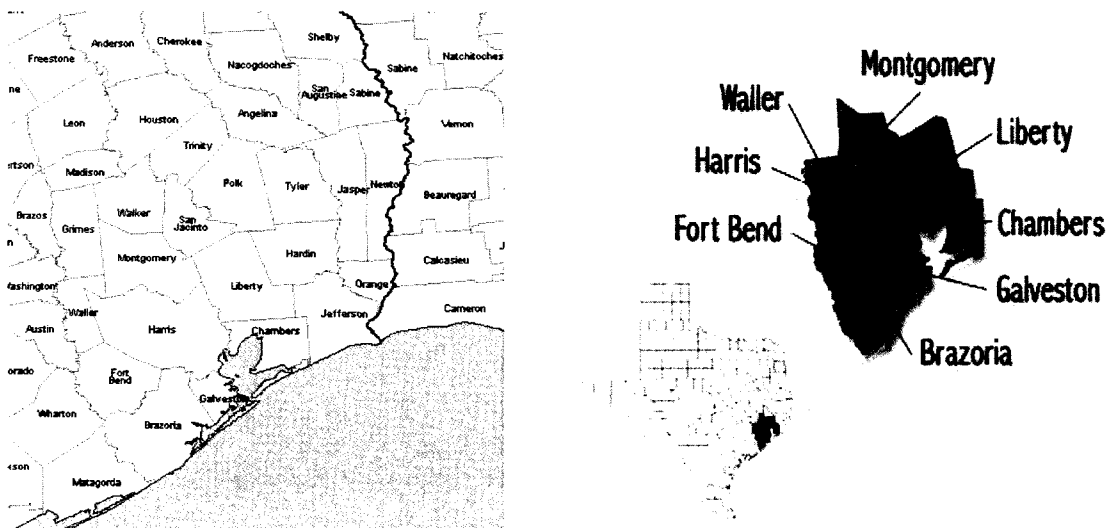


Figure 4.2: Eastern Texas county map (left) and HGB ozone non-attainment area (right).

(Source: TCEQ 2009)

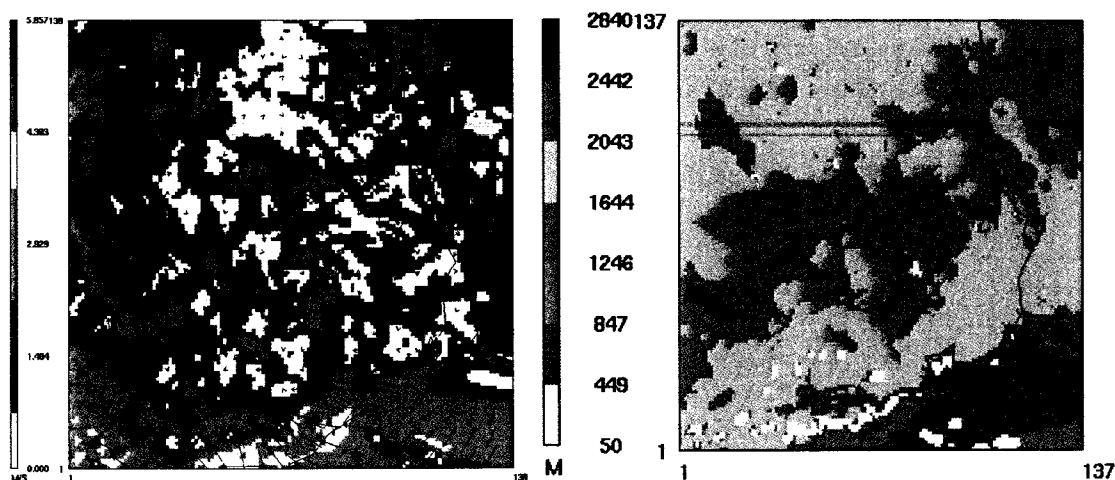


Figure 4.3: Wind conditions (left) and PBL height (right) at ozone peak time (4:00PM CST), August 31st, 2006.

The domain ozone distribution at the time of peak ozone for the episode for both EDDY and ACM2 schemes is shown in Figure 4.4.

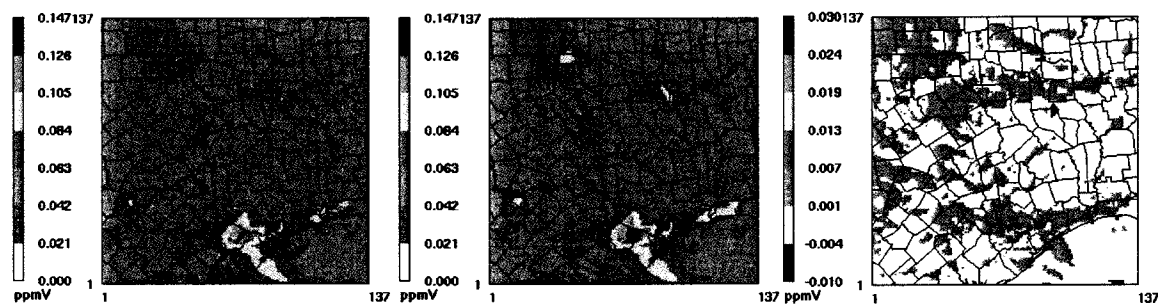


Figure 4.4: Ozone concentration at peak time (4:00PM CST), August 31st, 2006. (left) EDDY scheme; (middle) ACM2 scheme; (right) Difference (ACM2-EDDY)

The maximum ozone occurs downwind of Houston in Fort Bend County at 4:00pm (Figure 4.2, 4.4) most probably due to the meteorological conditions at that time. The wind plot (Figure 4.3) indicates that at 4:00pm, the northeasterly wind transports the pollutants

from the Houston Ship Channel, where one of the largest petroleum industries in the US located, to the downwind area. It also indicates that the sea breeze transports the ozone from the sea to inland at that time and that the low wind speed in Fort Bend County causes pollutant accumulation. The high temperature and humidity in the afternoon also enhances the ozone formation. The difference of predicted ozone concentrations from two vertical diffusion schemes (Figure 4.4) also illustrates that the ACM2 scheme tends to predict more surface ozone than the EDDY scheme.

4.2.2 EDDY and ACM2 modeling data comparisons

The pollutant concentrations simulated by CMAQ with two different schemes are analyzed here. Figure 4.5 shows the comparisons of simulated ground level primary and secondary pollutants when using the EDDY or ACM2 schemes. Figure 4.6 shows the corresponding comparisons of vertical profiles.

The EDDY scheme tends to predict large concentrations of primary pollutants (CO , NO_x) but smaller concentrations of secondary pollutants (O_3) at the surface compared to the ACM2 scheme (Figure 4.5). One possible reason is that the ACM2 scheme has faster vertical mixing under the convective boundary layer, leading to enhanced vertical transport of emitted primary pollutants. However, the EDDY scheme tends to predict smaller O_3 concentration near the surface than the ACM2 scheme, most probably due to more NO_x ($\text{NO} + \text{NO}_2$) being predicted at surface, leading to increased O_3 titration (Pleim 2009).

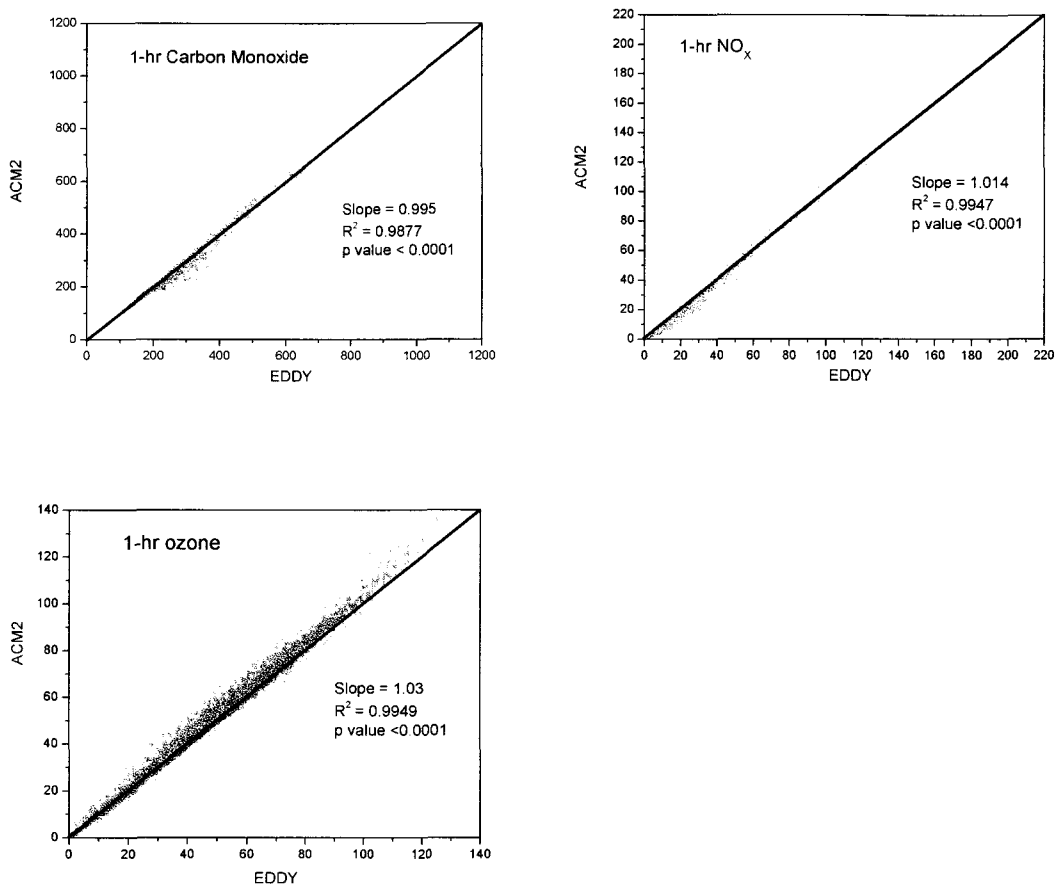
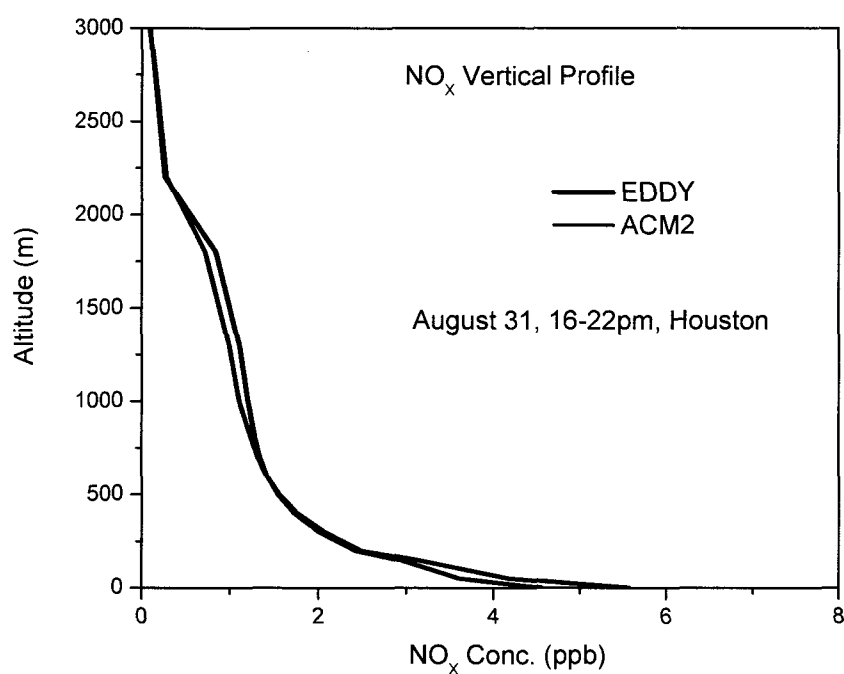


Figure 4.5: Regression between 1-hr average pollutant concentrations for all days in the episode modeled using EDDY and those modeled using ACM2.

Figure 4.6 shows the comparisons of vertical profiles produced by the EDDY and ACM2 schemes for NO_x and O_3 mixing ratios averaged over 4pm to 10pm on August 31st, 2006, in Houston. The ACM2 scheme has a more well-mixed profile under a convective PBL than EDDY because ACM2 considers turbulent diffusion under the PBL, making mixing more rapid than EDDY. The EDDY scheme has a deeper mixing depth than ACM2 because the EDDY scheme uses a quadratic height function to calculate eddy diffusivity, while the

ACM2 scheme uses a cubic height function (Pleim, 2009). In addition, EDDY tends to predict more NO_x near the surface, but less NO_x aloft than ACM2, most probably due to the faster upward mixing feature in ACM2 scheme causing smaller mixing ratios at surface but larger mixing ratios aloft. Again, the ACM2 scheme produces more O_3 than EDDY scheme under the PBL. In addition to the NO_x titration reason discussed above, another possible reason is that NO_x in ACM2 is better mixed than EDDY under the PBL, making more ozone yields.



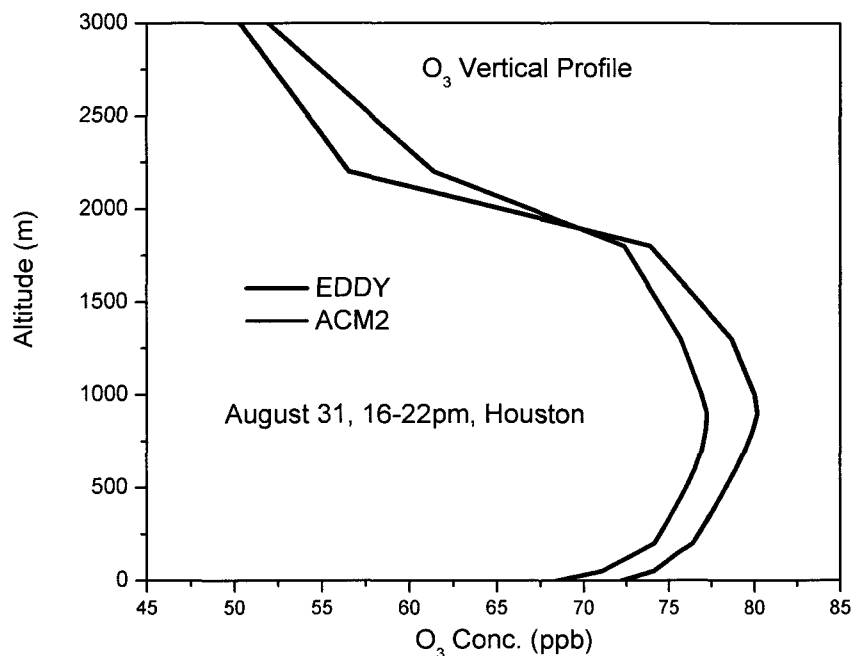


Figure 4.6: Vertical profiles produced by the EDDY and ACM2 schemes for NO_x (top) and O₃ (bottom) mixing ratios averaged over 4pm to 10pm on August 31st, 2006 in Houston.

4.2.3 Comparison with surface measurements

The comparisons of modeled O₃, NO_x and CO concentration with surface measurement data are presented in this section. Figure 4.7 shows the scatter plots of modeled ground level 1-hr average ozone versus measured 1-hr surface ozone for the whole episode at all ground measurement sites shown in Figure 3.3, in the domain.

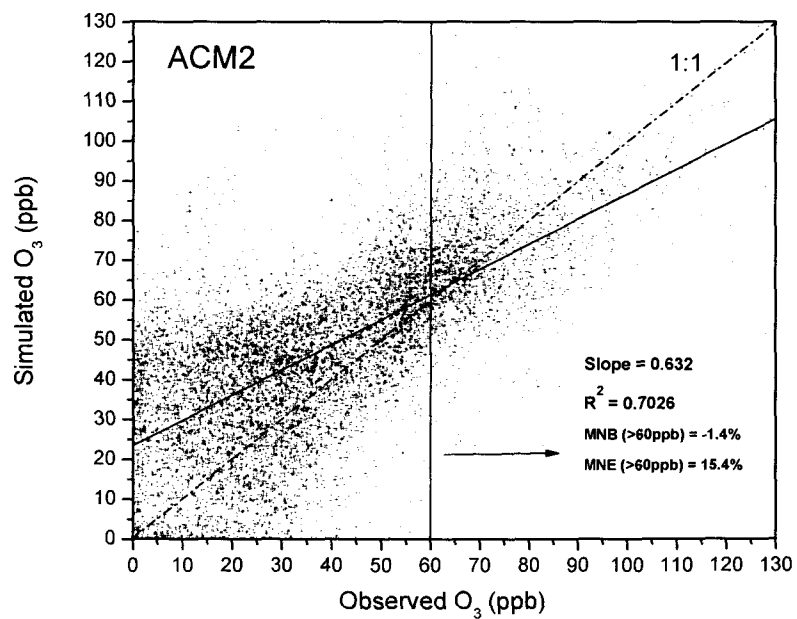
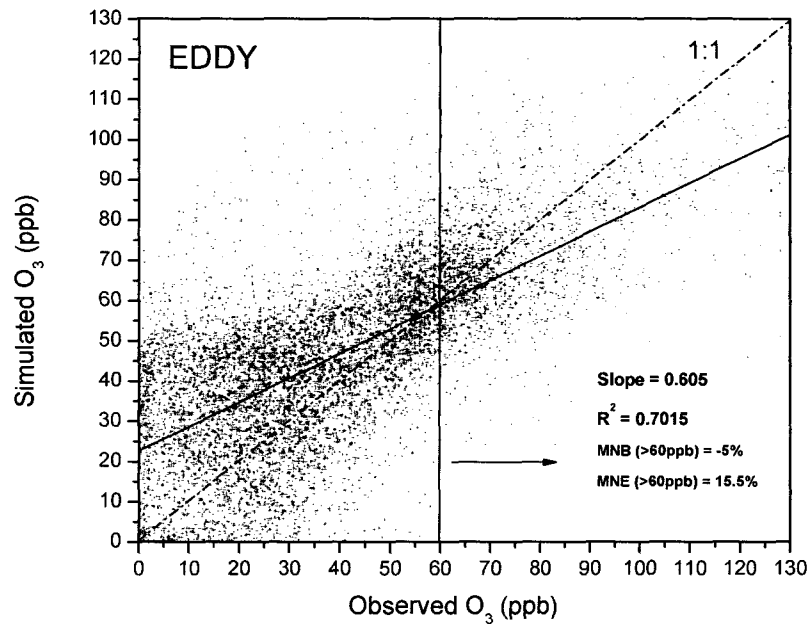


Figure 4.7: Scatter diagram of modeled 1-hr O₃ versus observed data, (top) EDDY, (bottom) ACM2.

Both vertical diffusion schemes simulated O_3 quite well generally, as correlation coefficients approach 0.7 (Figure 4.7). However, Figure 4.7 shows that the model performed weakly in predicting both very small and very large O_3 concentration in this case. The mean normalized bias (MNB) and mean normalized error (MNE) also have been calculated for the O_3 concentration value greater than 60 ppb. It shows that the simulation results from ACM2 and EDDY are virtually identical.

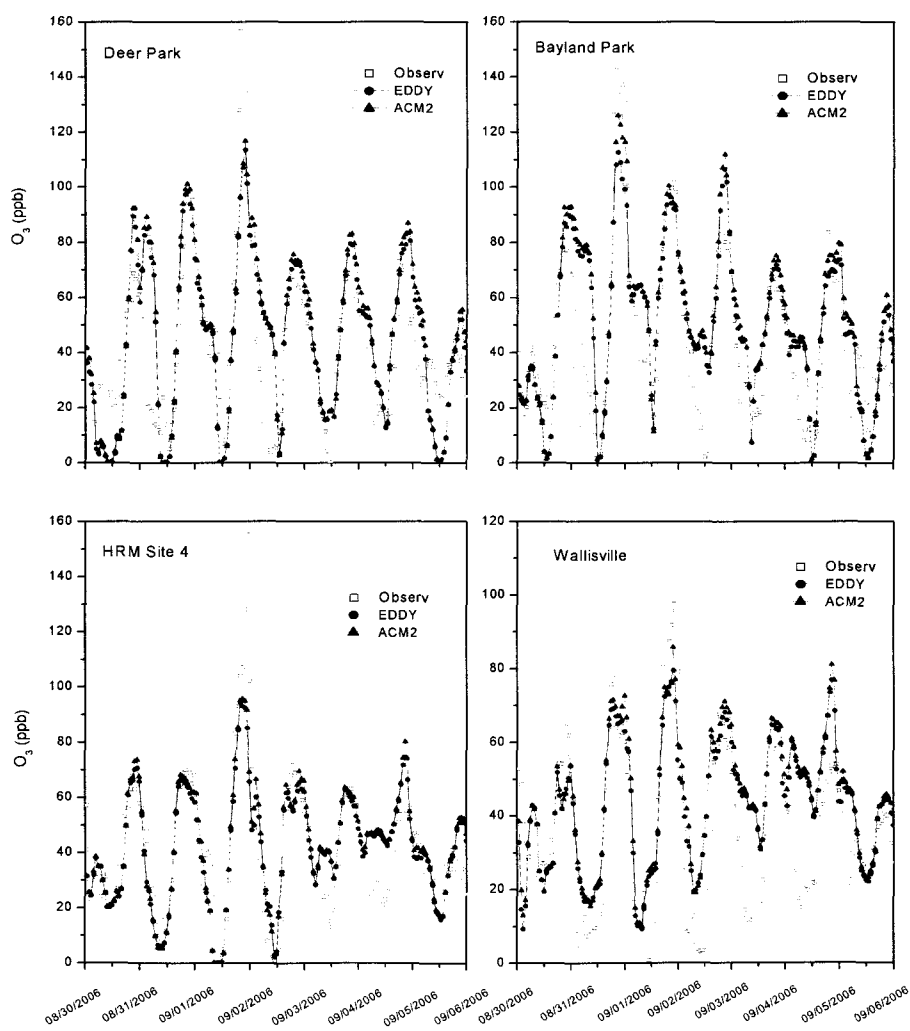


Figure 4.8: Time series (UTC) of predicted and observed ozone at four sites.

The temporal profiles of 1-hr average predicted and observed ozone at four measurement sites which have very high observed ozone concentration and inside the model domain, over seven days episode are shown in Figure 4.8, which indicate that the model mostly underpredicted the large daytime ozone concentrations (later afternoon) and overpredicted small nighttime ozone concentrations. The ACM2 scheme predicts larger ozone concentrations than the EDDY scheme, but the difference between the two schemes is small, averaging 2ppb and with a maximum value of 6ppb.

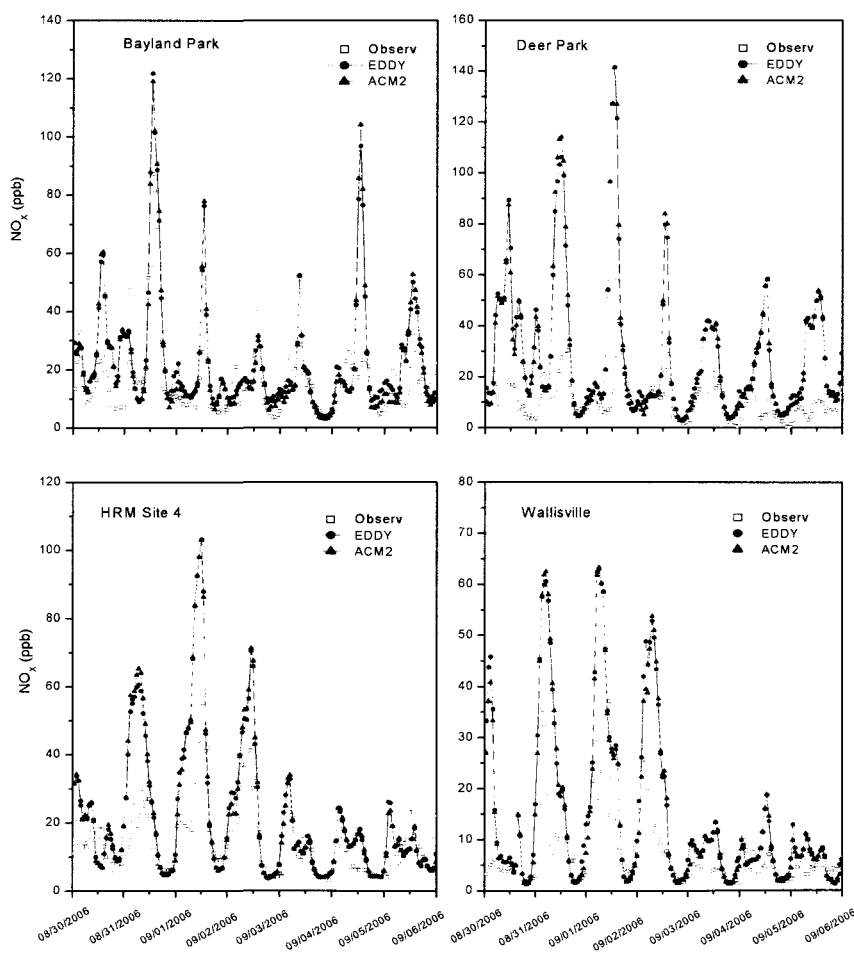


Figure 4.9: Time series (UTC) of predicted and observed NO_x at four sites.

The 1-hr average predicted and observed NO_x ($\text{NO} + \text{NO}_2$) at four measurement sites inside the model domain over seven days are shown in Figure 4.9, which indicate that both schemes simulated small NO_x concentration at nighttime very well, but significantly overpredicted peak daytime NO_x (early morning) at most sites. The ACM2 scheme predicts smaller NO_x concentration than the EDDY scheme, but the difference between two schemes is small, averaging 1ppb, with a maximum value of 3ppb.

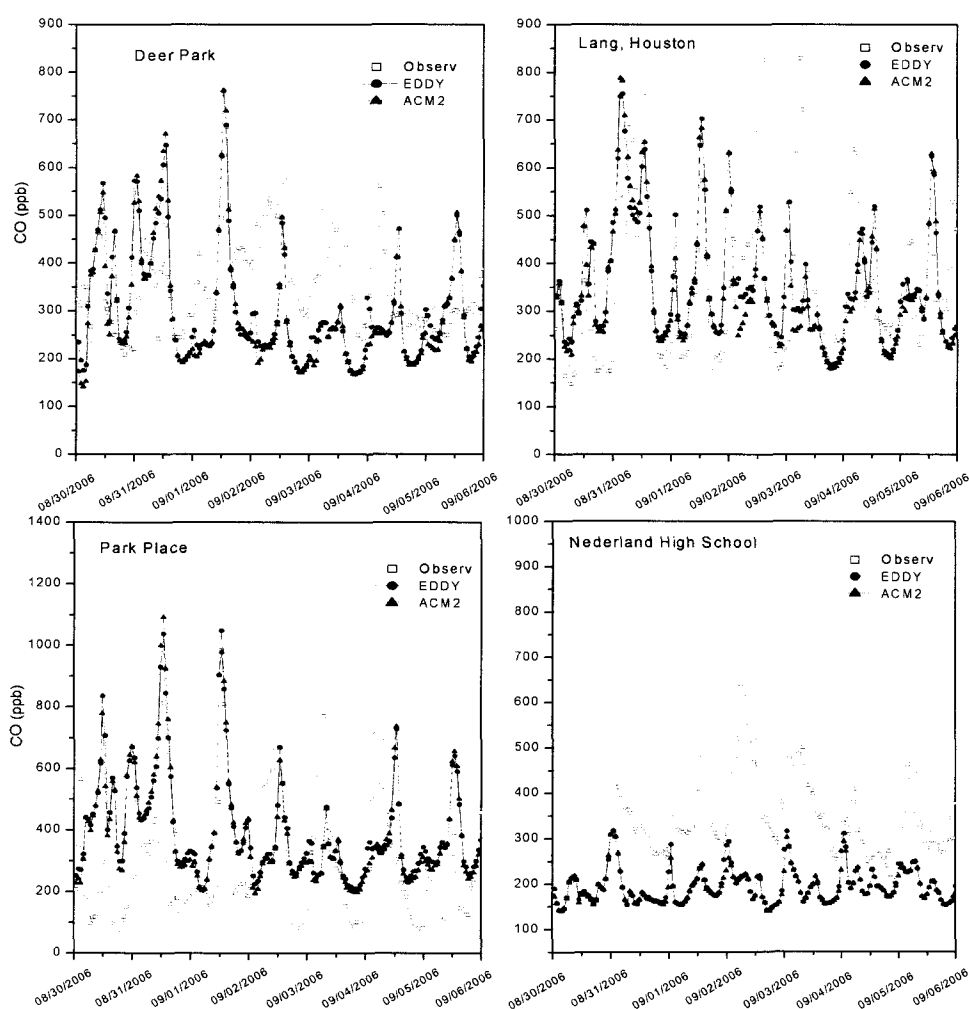


Figure 4.10: Time series (UTC) of predicted and observed CO at four sites.

Due to data availability, four measurement sites inside the model domain are chosen for the 1-hr average predicted and observed CO comparison (Figure 4.10), which indicates that both schemes performed poorly in simulating CO concentration. It shows that CO was significantly underpredicted at Deer Park and Nederland High School sites and that the simulations did not capture the largest and the smallest CO concentration at the Park Place and Lang sites. The ACM2 scheme predicts smaller CO concentration than the EDDY scheme, and the difference of simulated values between two schemes averages 30ppb, with a maximum value of 100ppb.

4.2.4 Comparison with ozonesonde measurements

Ten ozonesonde measurements made within the model domain were chosen for the vertical profiles comparisons. The data were obtained from Intercontinental Transport Experiment Ozonesonde Network Study 2006 (ION-6) campaign (Parrish et al., 2009). Six ozonesondes were launched at the University of Houston (UH), and four ozonesondes were launched from the NOAA R.H Brown vessel. Figure 4.11a shows measured and modeled data for six ozonesondes launched from UH. Figure 4.11b shows the corresponding information for the four ozonesondes launched from R.H Brown vessel.

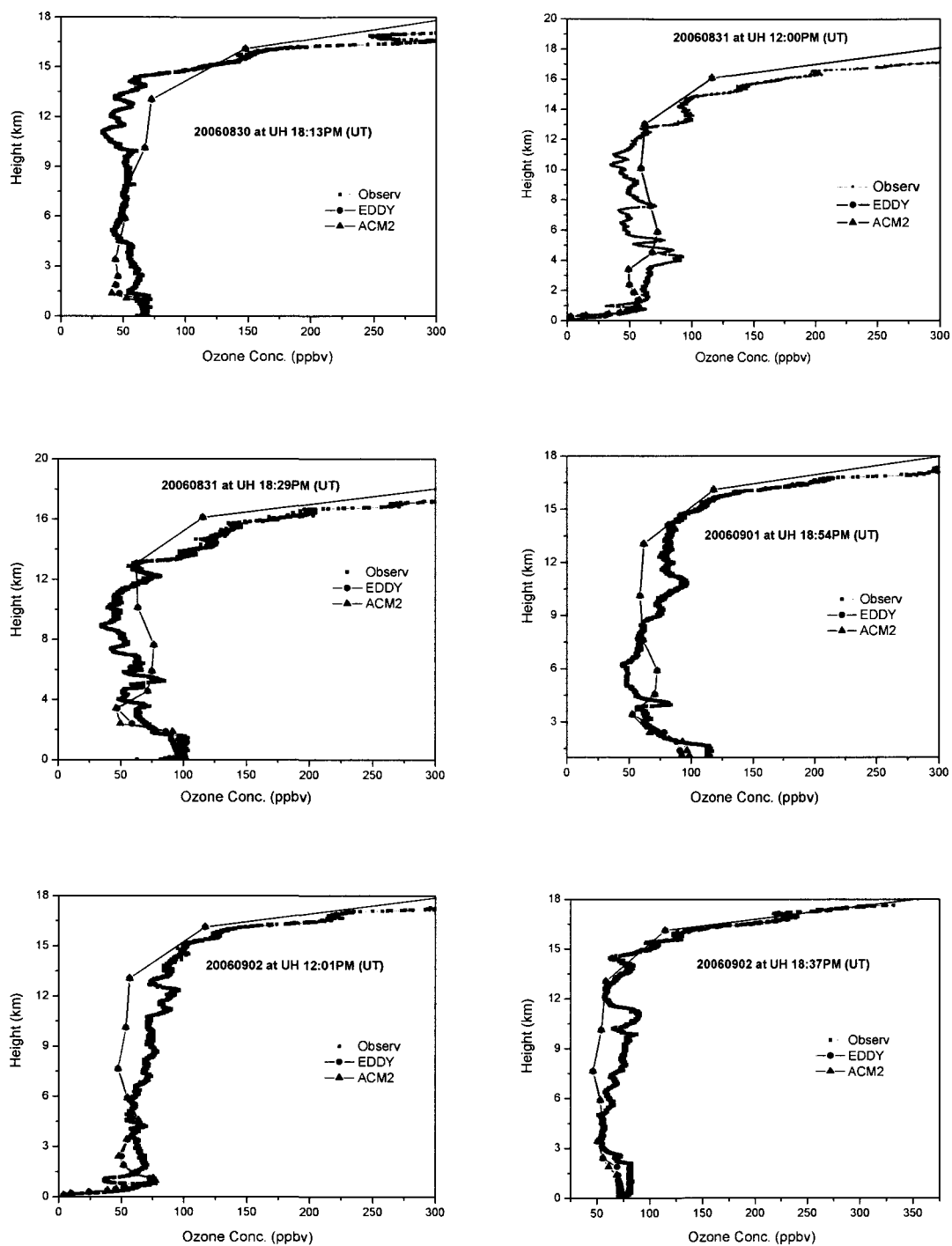


Figure 4.11a: Measured and modeled data for ozonesondes launched from University of Houston.

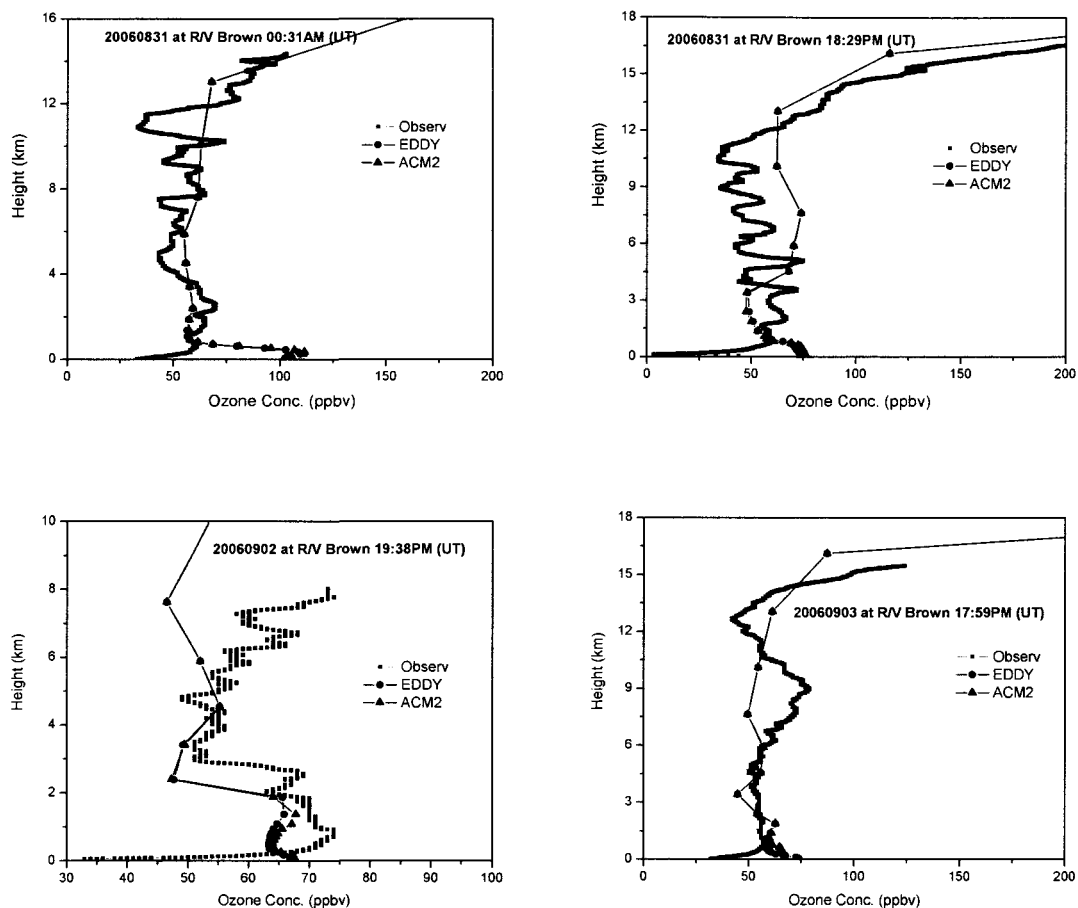


Figure 4.11b: Measured and modeled data for ozonesondes launched from R.H Brown.

Figure 4.11 shows that both vertical diffusion schemes in the model were capable of capturing the qualitative features of ozone vertical profiles measured by ozonesondes in each case. The ACM2 scheme continuously shows larger predicted ozone mixing ratios under the PBL, and the simulated vertical profiles by two schemes do not have significant difference above 3km. In Figure 4.11b, there are large discrepancies between modeled and observed profiles in the R.H Brown ozonesonde data. One possible reason is surface losses caused by measurement uncertainty (G.A. Morris, personal communication, 2009). In

addition, sudden increase of measured ozone concentration under the PBL shown in Figure 4.11a on August 31st and September 1st likely resulted from background ozone transported from both the continental and the sea (Rappengluck et al. 2008).

4.2.5 Comparison with regional aircraft measurements

Aircraft measurements conducted by the NOAA WP-3D aircraft (Parrish et al., 2009) also are compared to modeling results. A part of the P-3 aircraft track measurement data collected at 3:00pm (CST) on August 31st, 2006, (Figure 4.12) from 500 meters to 3000 meters height were used for comparison. The chemical species O₃, NO, NO₂, and CO measured by aircraft during 20 minute periods from 3:00pm to 4:00pm with 1 second resolution were compared with the extracted 1-hr average modeling data from each grid cell that the aircraft passed through at the corresponding time.

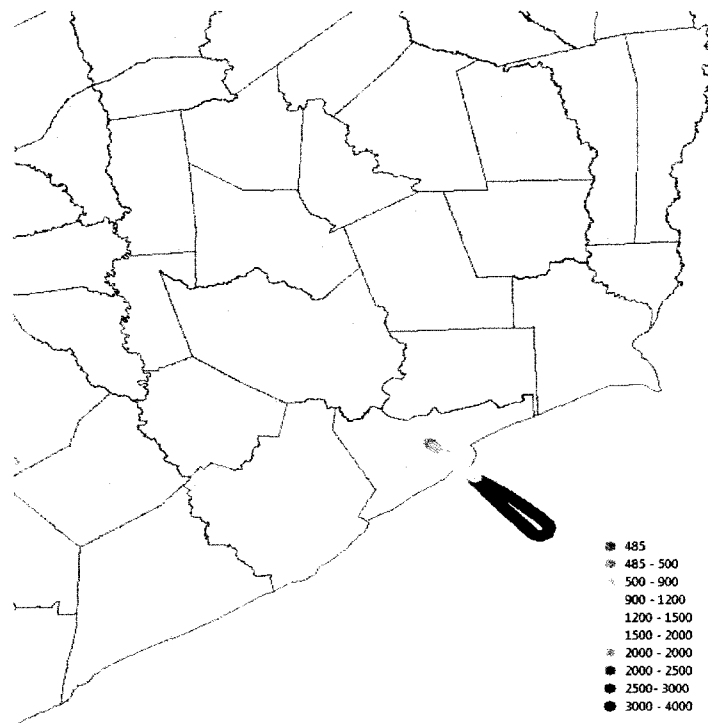
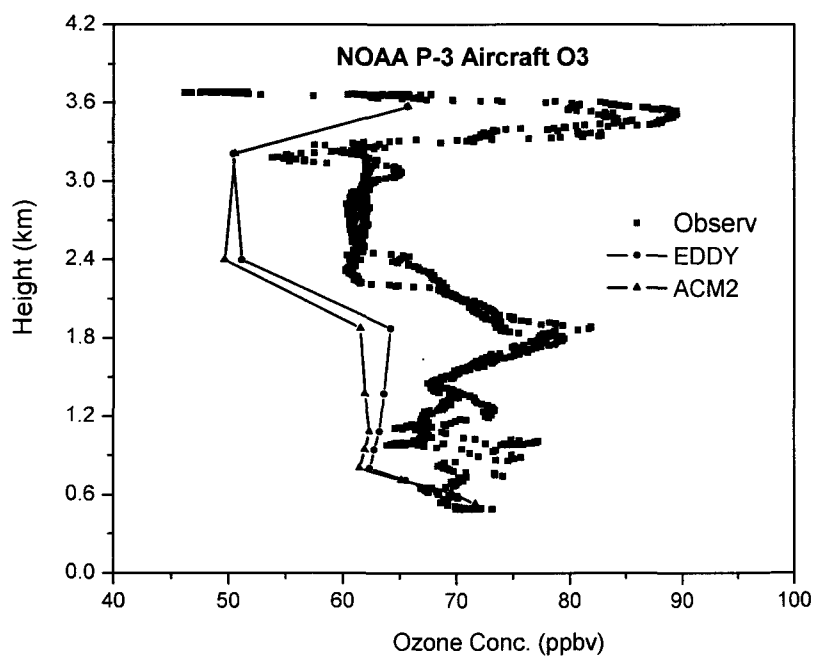


Figure 4.12: P-3 Aircraft track at 3:00pm on August 31st, 2006. (Color represents different altitude)



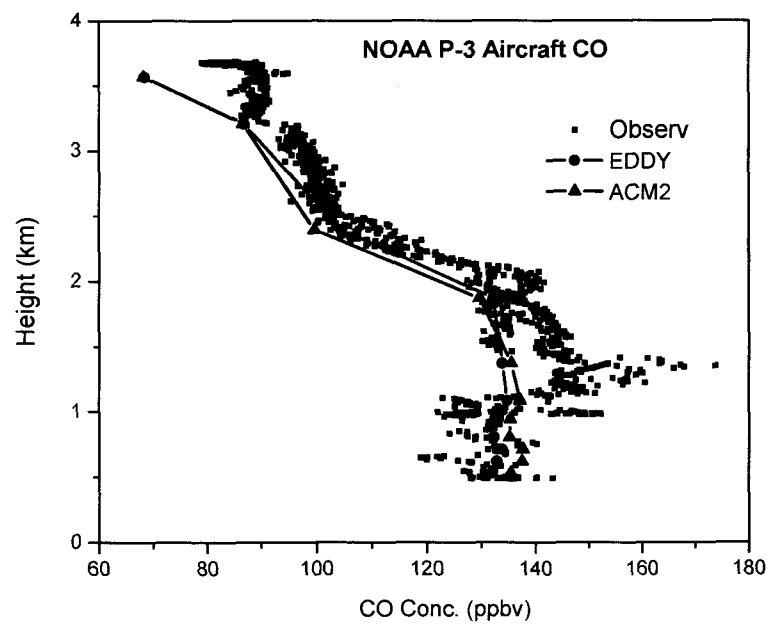
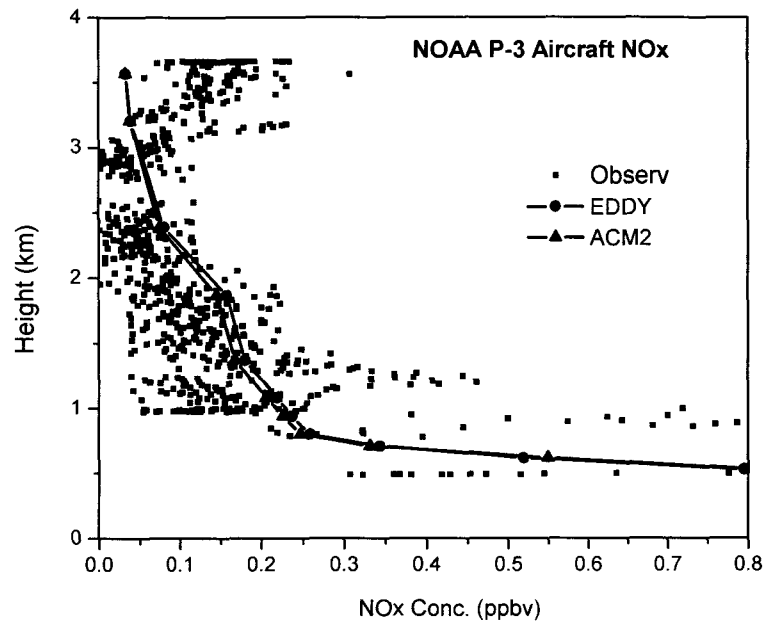


Figure 4.13: Modeled and P-3 aircraft data for O₃ (top), NO_x (NO+NO₂) (middle), and CO (bottom).

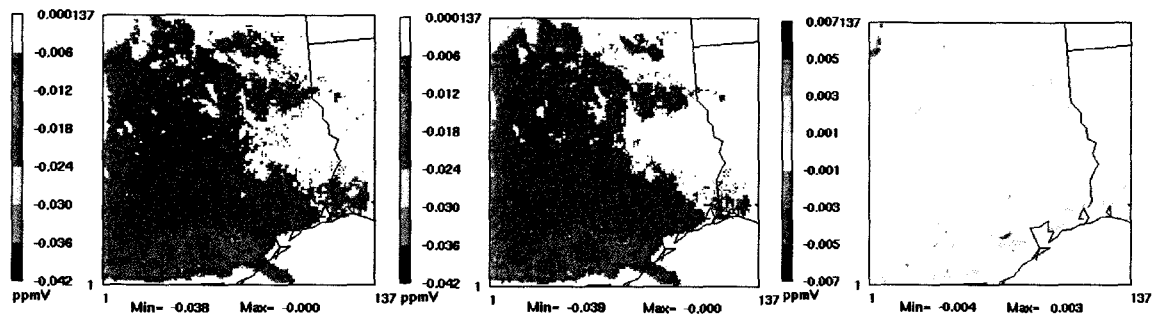
The modeled vertical profiles from both schemes virtually matched the observed ones quite well, especially for NO_x and CO modeling (Figure 4.13). The ACM2 scheme predicted larger concentrations of pollutant from 500m to the height of the PBL and predicted smaller concentrations of pollutant from the height of the PBL to 3km, and above 3km, there is no significant difference for the predicted concentrations between the EDDY and ACM2 schemes. The results are quite similar to those in Figure 4.6.

The discrepancies between modeled and observed data are much more significant than the differences between predicted concentrations using the two different vertical mixing schemes. Hence, the discrepancy between modeled and observed data cannot be rectified by changing the vertical mixing scheme. It is also not possible to determine which scheme is better on the basis of comparing modeling and observations.

4.3 Sensitivity analysis

The results of the analysis to determine the sensitivity of ozone to model input parameters are presented here. The first and second order ozone sensitivities to dry deposition velocity, to anthropogenic NO_x, and to anthropogenic VOC and the cross sensitivity of ozone to anthropogenic NO_x and anthropogenic VOC emission with dry deposition velocity were calculated by CMAQ-DDM. The DDM results are illustrated below.

$\partial[O_3]/\partial \epsilon_{V_{depl}}$ (ozone sensitivity to dry deposition velocity of all species)



$\partial^2[O_3]/\partial \epsilon_{V_{depl}}^2$ (second order ozone sensitivity to dry deposition velocity)

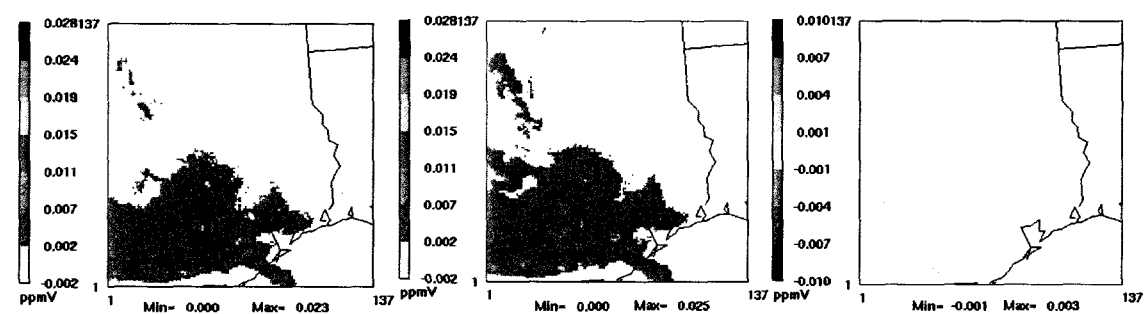


Figure 4.14a: Ozone sensitivity to dry deposition velocity at 4:00pm CST on August 31st, 2006. (left) EDDY, (middle) ACM2, (right) difference (ACM2-EDDY)

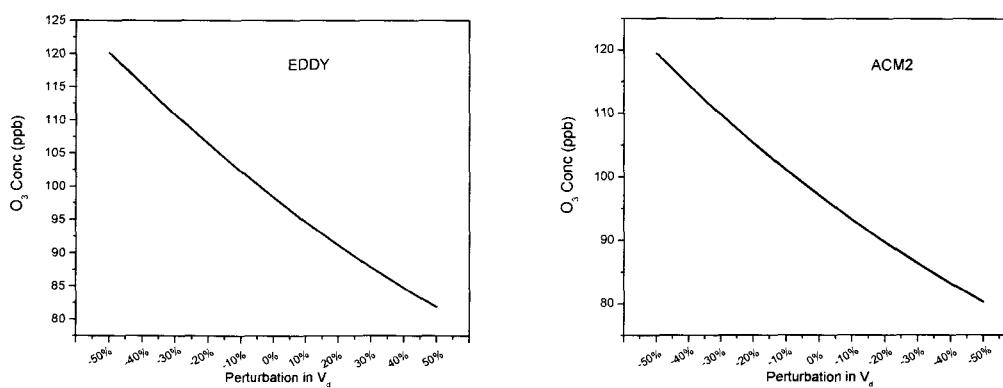


Figure 4.14b: Responsiveness of ozone to dry deposition velocity at 4:00pm CST.

The first order ozone sensitivity to dry deposition velocity (Figure 4.14a) is negative because enhanced dry deposition velocity decreases atmospheric concentrations. The second order ozone sensitivity to dry deposition velocity (Figure 4.14a) is positive because of the convex response of ozone to dry deposition velocity at that time (Figure 4.14b). It also indicates that the nonlinearity in ozone response caused by dry deposition velocity is small.

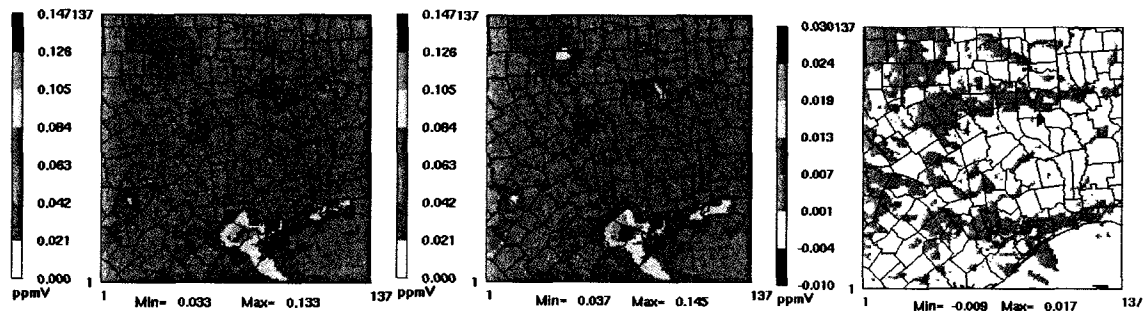
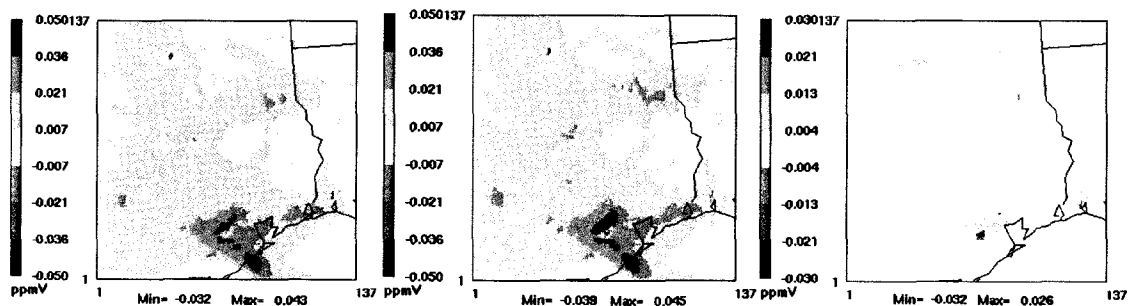
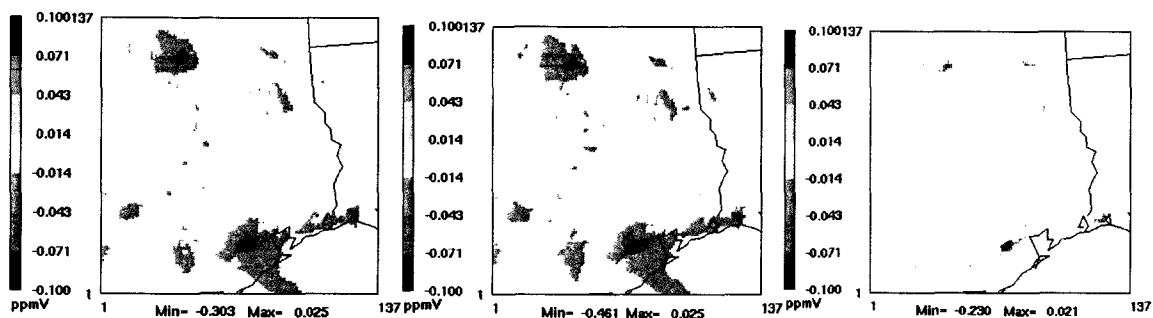


Figure 4.15a: Ozone concentration at peak time (4:00PM CST), August 31st, 2006. (left) EDDY scheme; (middle) ACM2 scheme; (right) Difference (ACM2-EDDY)

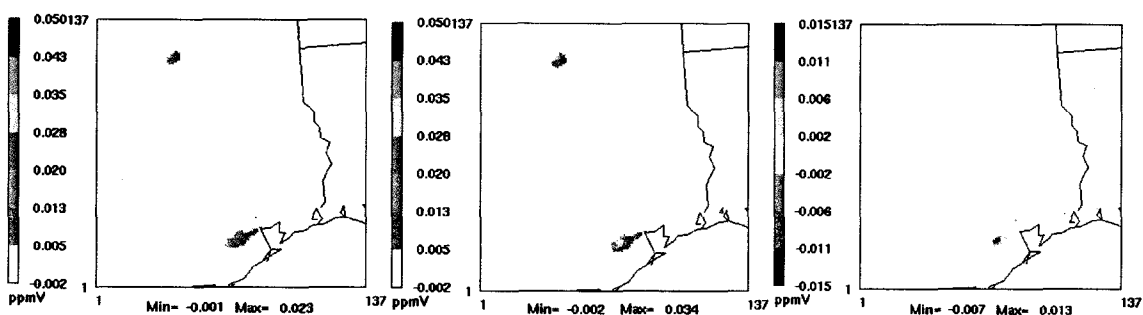
$\partial[O_3]/\partial \epsilon_{E,NO_x}$ (ozone sensitivity to anthropogenic NO_x emission)



$\partial^2[O_3]/\partial \epsilon_{E,NO_x}^2$ (second order ozone sensitivity to anthropogenic NO_x emission)



$\partial[O_3]/\partial \epsilon_{E,VOC}$ (ozone sensitivity to anthropogenic VOC emission)



$\partial^2[O_3]/\partial \epsilon_{E,VOC}^2$ (second order ozone sensitivity to anthropogenic VOC emission)

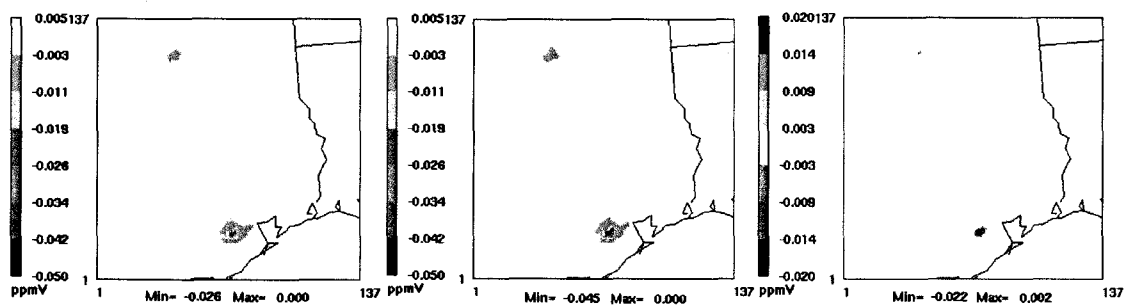


Figure 4.15b: Ozone sensitivities to anthropogenic NO_x and VOC at peak time (4:00PM CST), August 31st, 2006. (left) EDDY scheme; (middle) ACM2 scheme; (right) Difference (ACM2-EDDY)

The maximum ozone concentration occurs downwind of Houston in Fort Bend County at 4:00pm (Figure 4.15a). From the Figure 4.15b, the first order ozone sensitivity to anthropogenic NO_x , $\partial[\text{O}_3]/\partial \epsilon_{E,\text{NO}_x}$, is negative indicating that VOC control will be effective for ozone reduction in that area and at that time (how to distinct control region has already been discussed in Chapter Three). The response of ozone calculated from the ACM2 scheme (Figure 4.15b) seems to be more sensitive to anthropogenic NO_x and VOC than the EDDY scheme, indicating that different emission controls may be designed as different vertical diffusion schemes are used. Compared with the first order sensitivities, the second order sensitivities become more localized. The second order ozone sensitivity to anthropogenic NO_x , $\partial^2[\text{O}_3]/\partial \epsilon_{E,\text{NO}_x}^2$, shows predominantly negative value indicating large nonlinear and concave response of ozone. The second order ozone sensitivity to anthropogenic VOC, $\partial^2[\text{O}_3]/\partial \epsilon_{E,\text{VOC}}^2$, shows a much smaller magnitude than $\partial^2[\text{O}_3]/\partial \epsilon_{E,\text{NO}_x}^2$ indicating less degree of nonlinearity in ozone response (Hakami et al., 2004; Cohan et al., 2005).

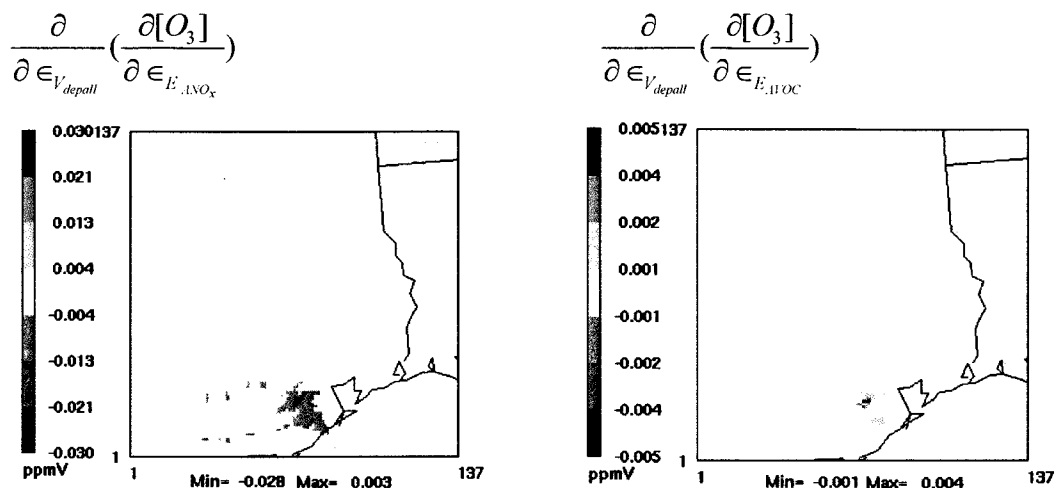


Figure 4.16: Cross sensitivity coefficients of ozone to dry deposition velocity and anthropogenic NO_x (left), and anthropogenic VOC (right) at 4:00pm on August 31st, 2006.

The cross sensitivity coefficients calculated by the EDDY scheme are shown in Figure 4.16. The result from the ACM2 scheme is not shown because it was not reliable as discussed in Section 4.1. The cross sensitivity of ozone to anthropogenic NO_x emission and dry deposition velocity shows negative value at that time, indicating that if dry deposition velocities for all species are underpredicted, ozone becomes more sensitive to ANO_x . In contrast, the cross sensitivity of ozone to anthropogenic VOC emission and dry deposition velocity shows positive value at that time, indicating that if dry deposition velocities for all species are underpredicted, ozone becomes less sensitive to AVOC . The magnitude of cross sensitivity coefficients are much smaller than the first order and second order sensitivities as showed above, but these terms will become much important in uncertainty analysis as discussed below.

4.4 Uncertainty analysis in dry deposition velocity

As described in Chapter Two, recent studies indicate that the uncertainty in dry deposition velocities could be as large as $\pm 30\%$ (Wesely and Hicks 2000). Therefore, it is essential to analyze the impact of uncertainty in dry deposition velocity on model performance. The effects of uncertainty in dry deposition velocity on model simulation and on emission control are discussed here.

4.4.1 Effect on model simulations

Based on equation 3.15, the effect of $\pm 30\%$ uncertainty in dry deposition velocity for all depositing species on model simulation results can be quantified. The effects of uncertainty in dry deposition velocities on surface ozone modeling and on ozone, sulfur dioxide, and nitric acid simulated vertical profiles are evaluated in Figure 4.17 and 4.18, respectively.

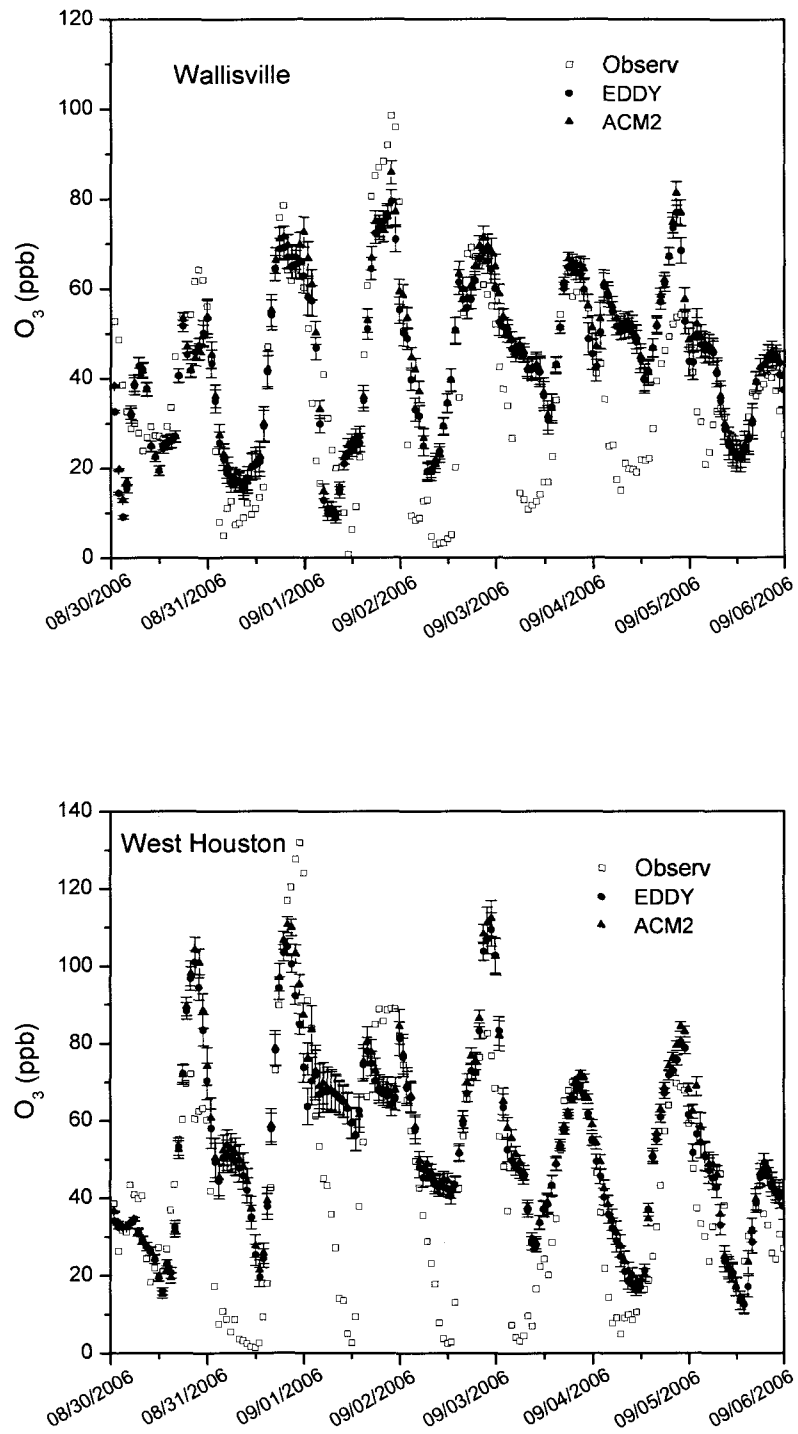


Figure 4.17: Effect of uncertainty in O₃ dry deposition velocity on surface O₃ modeling.

As discussed above, when the dry deposition velocities decrease, the species concentrations increase. The higher and lower error bars in Figure 4.17 represent ozone concentration adjusted by -30% and +30% uncertainties in dry deposition velocity. The results indicate that compared to the discrepancy between modeled and observed results, the effect of uncertainty in dry deposition velocity on simulated surface O_3 is small.

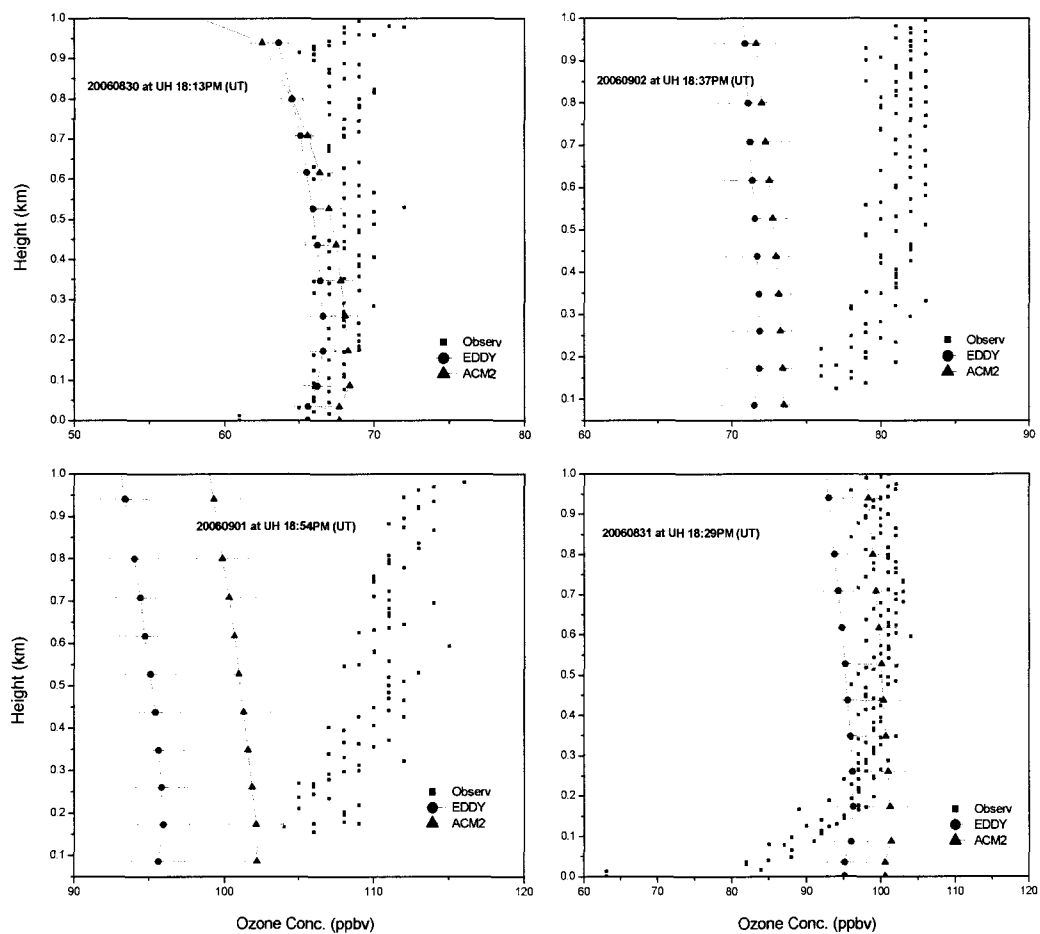


Figure 4.18a: Effect of uncertainty in dry deposition velocity on O_3 vertical profile.

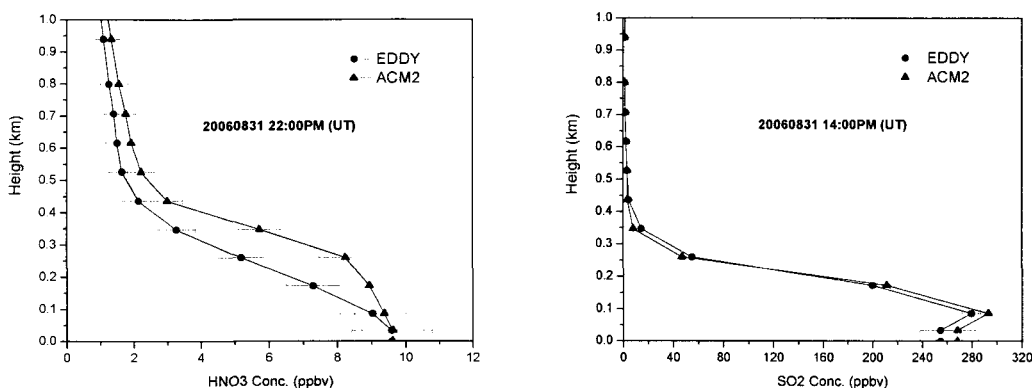


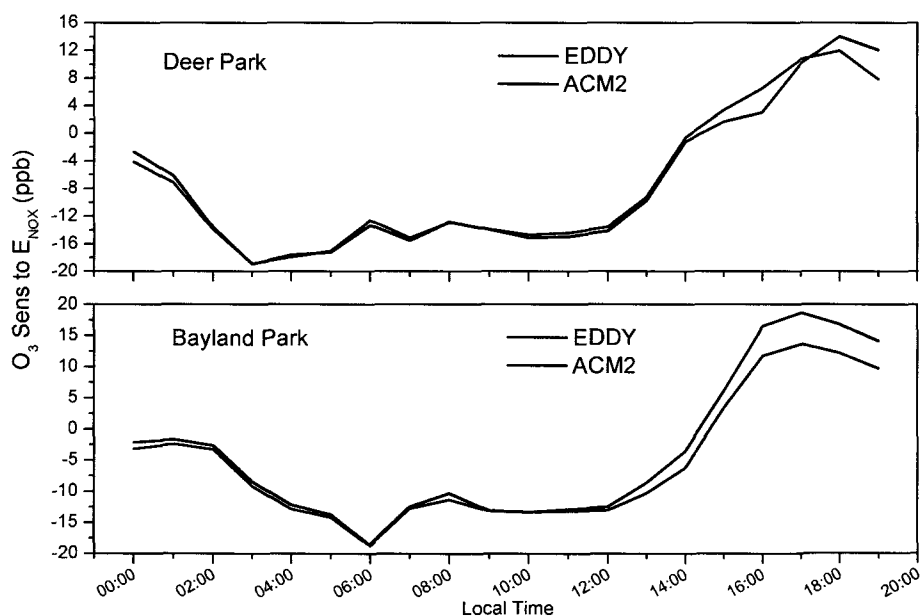
Figure 4.18b: Effects of uncertainty in dry deposition velocities on HNO₃ (left) and SO₂ (right) vertical profiles.

However, Figure 4.18a illustrates that considering the uncertainty in O₃ dry deposition velocity may make the modeled O₃ vertical profile closer to the observed values after adjusting the profile, but the uncertainty in O₃ dry deposition velocity is certainly not the driving force causing the discrepancy between modeled and observed profile in this case. However, Figure 4.18b demonstrates that for species with larger dry deposition velocity, such as HNO₃ or SO₂, the effect of uncertainty in dry deposition velocity on modeled results at lower layer is more significant.

4.4.2 Effect on emission control strategy

As discussed in chapter 3, uncertainties in inputs such as dry deposition velocities can influence the sensitivity of ozone to NO_x and VOC emission controls. Based on the equations 3.19 and 3.20 derived in chapter 3, the effect of dry deposition velocity on

emission control strategy can be evaluated. Figure 4.19 shows the effect of uncertainty in choosing different vertical mixing schemes on both NO_x and VOC emission controls, and Figure 4.20 shows the effect of uncertainty in dry deposition velocity on both NO_x and VOC emission controls, at the Bayland Park and Deer Park ozone monitoring sites in Houston. The Bayland Park site is in a suburban area in the west of Houston, and the Deer Park site is in the Ship Channel area in the east of Houston. Both sites have predicted future ozone designed values that exceed 84 ppb (TCEQ 2009). The average hourly sensitivity coefficients of ozone to NO_x and VOC emission were calculated for the 7-day episode in this case.



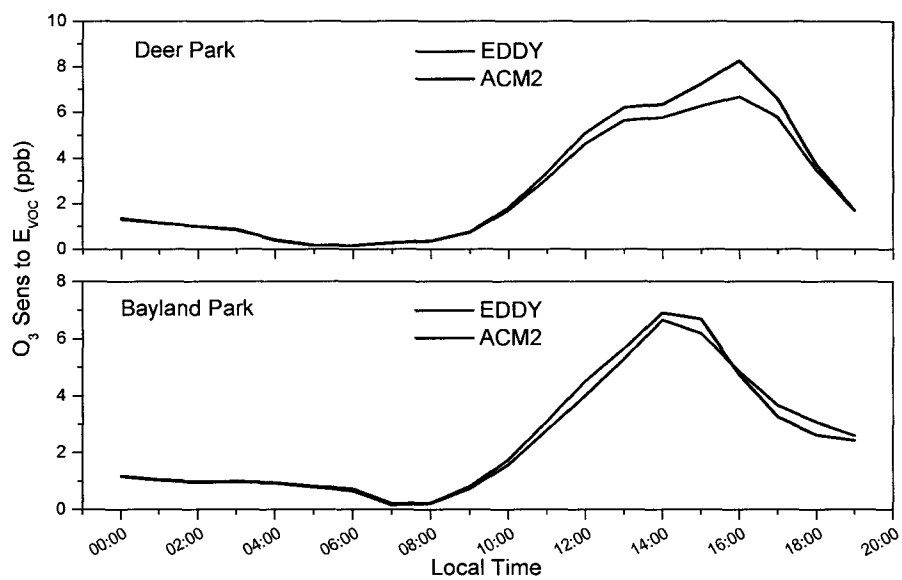
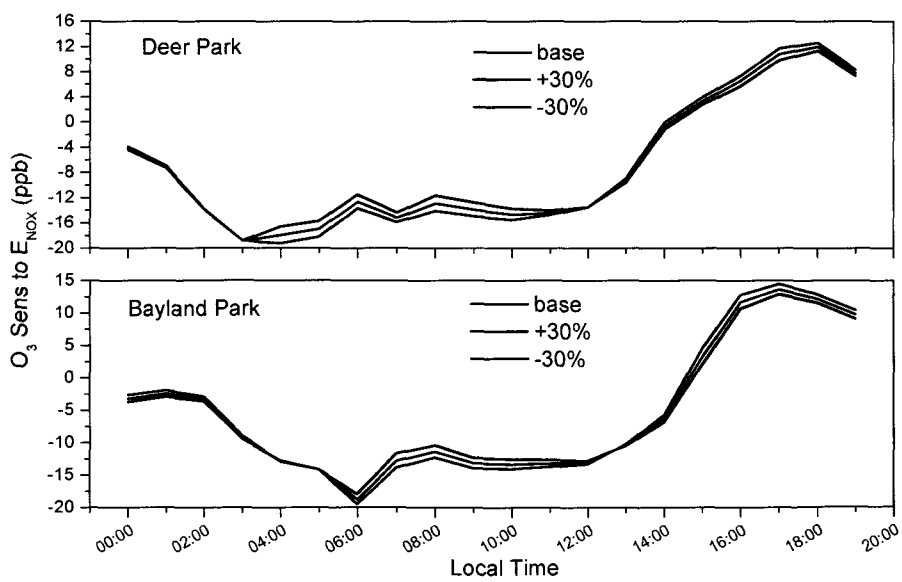


Figure 4.19: Effects of uncertainty in different vertical mixing schemes on O₃ sensitivity to anthropogenic NO_x (top) and to anthropogenic VOC (bottom) emissions.



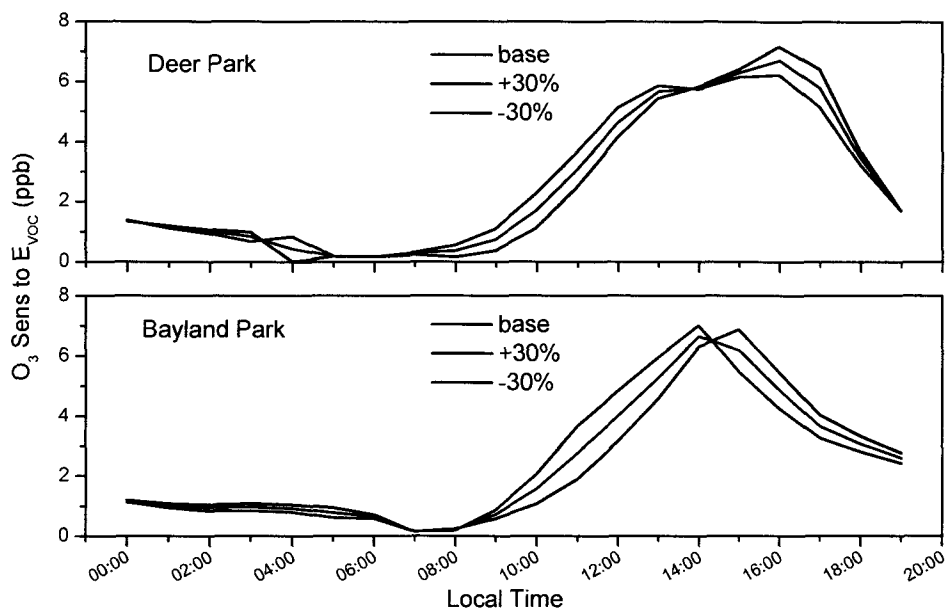


Figure 4.20: Effects of uncertainty in dry deposition velocity on O_3 sensitivity to anthropogenic NO_x (top) and to anthropogenic VOC (bottom) emissions.

Table 4.2: Effects of uncertainties on emission control (Deer Park)

Emission Control	EDDY scheme	ACM2 scheme	EDDY with Vd +30%	EDDY with Vd -30%
S^I (O_3 to NO_x) (ppb)	-3.97	-5.05	-4.23	-3.71
S^I (O_3 to VOC) (ppb)	4.96	5.62	4.88	5.03

Note: averaged over 10am-5pm (local time)

Table 4.3: Effects of uncertainties on emission control (Bayland Park)

Emission Control	EDDY scheme	ACM2 scheme	EDDY with Vd +30%	EDDY with Vd -30%
S ¹ (O ₃ to NO _x) (ppb)	-3.4	-1.2	-3.72	-3.17
S ¹ (O ₃ to VOC) (ppb)	4.37	4.57	4.18	4.57

Note: averaged over 10am-5pm (local time)

The first order sensitivity coefficients of ozone to anthropogenic NO_x and anthropogenic VOC used here can be considered as emission control factors. For example, if the first order ozone sensitivity to anthropogenic NO_x equals to 12ppb, then 1.2ppb ozone can be reduced by controlling 10% anthropogenic NO_x emission. Figure 4.19 indicates that the ANO_x and AVOC emission controls may vary significantly by using different vertical diffusion schemes, especially from 10am to 5pm. At both sites, generally, the ozone sensitivities calculated with the ACM2 scheme to anthropogenic NO_x and to anthropogenic VOC are more sensitive than those using the EDDY scheme (Table 4.2, 4.3), reflecting that at certain times, controlling the same amount of ANO_x and AVOC emissions may have less effect on predicted ozone reductions when the EDDY scheme is used in the model.

Figure 4.20 also indicates that the response of ozone to ANO_x and AVOC may vary temporally due to the uncertainty in dry deposition velocity. The average values of responses of ozone to ANO_x and AVOC with ±30% uncertainty in dry deposition velocity

showed in Table 4.2 and 4.3 indicate that, at the Bayland Park and Deer Park sites, the effect of uncertainty in dry deposition velocity on AVOC emission control is smaller than that on ANO_x emission control. The variation in ozone response to ANO_x could reach approximately 14% at Deer Park, and 17% at Bayland Park, and the variation in ozone response to AVOC could reach approximately 3% at Deer Park, and 9% at Bayland Park.

References

- Cohan D.S., Hakami, A., Hu, Y.T., and Russell, A.G. (2005) Nonlinear response of ozone to emissions: Source apportionment and sensitivity analysis. *Environmental Science and Technology*. 39, 6739-6748.
- Hakami, A., Odman, M.T., and Russell, A.G. (2003) High-order, direct sensitivity analysis of multidimensional air quality models. *Environmental Science and Technology*. 37, 2442-2452.
- Hakami, A., Odman, M.T., and Russell, A.G. (2004) Nonlinearity in atmospheric response: A direct sensitivity analysis approach. *Journal of Geophysical Research*. 109, D15303.
- Parrish, D.D., Allen, D.T., Bates, T.S., Estes, M., Fehsenfeld, F.C., Feingold, G., Ferrare, R., Hardesty, R.M., Meagher, J.F., Nielsen-Gammon, J.W., Pierce, R.B., Ryserson, T.B., Seinfeld, J.H. and Williams, E.J. (2009) Overview of the second Texas Air Quality Study (TexAQS II) and the Gulf of Mexico Atmosphere Composition and Climate Study (GoMACCS). *Journal of Geophysical Research*. 114, D00F13.
- Pleim, J.E. (2006) A new combined local and non-local PBL model for meteorology and air quality modeling. CMAS conference paper. North Carolina.

Rappengluck, B., Perna, R., Zhong, S., and Morris, G.A. (2008) An analysis of the vertical structure of the atmosphere and the upper-level meteorology and their impact on surface ozone levels in Houston, Texas. *Journal of Geophysical Research*. 113, D17315.

TCEQ. *Houston-Galveston-Brazoria Ozone Nonattainment Area*.

(<http://www.tceq.state.tx.us/implementation/air/sip/hgb.html#project> Accessed on October 1st, 2009)

TCEQ. *Proposed HGB Attainment Demonstration SIP Revision for the 1997 Eight-Hour Ozone Standard*.

(<http://www.tceq.state.tx.us/implementation/air/sip/hgb.html#project> Accessed on November 23rd, 2009)

Wesely, M.L. and Hicks, B.B. (2000) A review of the current status of knowledge on dry deposition. *Atmospheric Environment*. 34, 2261-2282.

CHAPTER 5

Conclusions and Recommendations

A study on the influence of uncertainties in vertical mixing algorithms on photochemical air quality model was carried out in this thesis. It includes three major parts: model development, model evaluation, and model application. In the model development part, the first and second order of dry deposition velocity and eddy diffusivity sensitivities were implemented into CMAQ-DDM for both EDDY and ACM2 vertical diffusion schemes. In the model evaluation part, the performance of two vertical diffusion schemes was evaluated by comparing with field campaign measurement data. In the model application part, the sensitivity and uncertainty analysis by using the newly implemented code were conducted.

5.1 Conclusions

Seven main conclusions could be drawn from this study:

1. DDM was successfully implemented into ACM2 scheme in CMAQ.
2. The first and second order dry deposition velocity and eddy diffusivity sensitivities were implemented into DDM for both EDDY and ACM2 schemes in CMAQ successfully. Comparison with Brute Force approximation approach shows that the results from two methods are in very good agreement. The cross sensitivity term in ACM2 scheme was not reliable and needs further investigation.

3. Comparisons between modeling results from two schemes indicated that the ACM2 scheme tends to predict larger concentrations of secondary pollutants and smaller concentrations of primary pollutants at the surface compared to the EDDY scheme; the ACM2 scheme has a more well-mixed profile under the PBL, and the EDDY scheme has a deeper mixing depth.
4. Based on comparisons between modeled and observed data, both schemes performed well in simulating surface ozone concentration but performed poorly in simulating surface NO_x and CO concentrations. They both are capable of capturing the qualitative features of vertical profiles measured by ozonesonde and aircraft. However, at the surface level, the model performed weakly in simulating the very large and very small pollutant concentrations in this case. The discrepancies between modeled and observed data are much more significant than the differences of predicted concentrations between the two vertical mixing schemes. Hence, the discrepancy between modeled and observed data cannot be explained by changing the vertical mixing schemes. It is also not possible to determine which scheme is better on the basis of comparing modeled and observed data.
5. Sensitivity analysis results show that the chemical processes dominate the nonlinearity in the ozone responsiveness and that the largest nonlinear responsiveness of ozone was produced by anthropogenic NO_x . The responsiveness of ozone to dry deposition velocity and to anthropogenic VOC is less nonlinear than that to the anthropogenic

NO_x emission.

6. The effect of uncertainty in dry deposition velocities on ozone simulation results is small compared to the discrepancy between modeled and observed O₃ concentrations in this case. It may have significant impact on the modeling of pollutants with large dry deposition velocity, such as HNO₃ and SO₂.
7. The uncertainty in dry deposition velocity may cause as large as 60% variation in responsiveness of ozone to emission control. Different vertical diffusion schemes could have even more impact on emission control strategy.

5.2 Recommendations for future work

A few recommendations are suggested for future work.

1. As mentioned in Chapter Four, the newly implemented DDM code for calculating dry deposition velocity and eddy diffusivity sensitivities only had accurate results in fine resolution model grids (less than 8km) with convective cloud process turned off. Hence, the convective cloud process in the CMAQ-DDM model needs to be improved for better accuracy in DDM calculation of dry deposition velocity and eddy diffusivity sensitivities.
2. Further investigations and evaluations are needed for the second order sensitivity coefficients of dry deposition velocity calculations in the ACM2 scheme. The second order term for eddy diffusivity also needs to be tested and evaluated.

3. As mentioned in Chapter Three, the uncertainty analysis in eddy diffusivity was not performed in this study because a model inconsistency error between MM5 and CMAQ may occur in the simulation. Therefore, the sensitivity code also may need to be implemented into the meteorological model in order to investigate the effect of uncertainty in eddy diffusivity on model performance more realistically.
4. The evaluations of the uncertainty in choosing different vertical diffusion schemes and in dry deposition velocity on emission controls were only performed for two sites and the results are different. Hence, more evaluations need to be conducted. For example, more sites under different control regions can be investigated, including considering the effect on 8-hr ozone control strategy.
5. The results from this study showed that the uncertainties in dry deposition velocity and eddy diffusivity in the simulations cannot be ignored. Hence, the inverse modeling technique could be used in the future work to adjust the dry deposition velocity and eddy diffusivity in the simulation. For example, we can use the calculated sensitivity coefficients of dry deposition velocity and eddy diffusivity by DDM in the inverse modeling framework to minimize the difference between modeled and observed data, and therefore to optimize the input dry deposition velocity and eddy diffusivity values.